

Pre-assembled GPCR signaling complexes mediate unique cellular responses to ultra-low ligand concentrations

Srgjan Civciristov¹, Andrew M. Ellisdon², Ryan Suderman³, Cindy K. Pon¹, Bronwyn A. Evans¹, Oded Kleifeld^{2,4}, Steven J. Charlton^{5,6}, William S. Hlavacek³, Meritxell Canals¹, Michelle L. Halls^{1,*}

¹Drug Discovery Biology Theme, Monash Institute of Pharmaceutical Sciences, Monash University, Parkville, Victoria 3052, Australia.

²Biomedicine Discovery Institute and Department of Biochemistry and Molecular Biology, Monash University, Clayton, Victoria 3800, Australia.

³Theoretical Biology and Biophysics Group, Theoretical Division and Center for Nonlinear Studies, Los Alamos National Laboratory, Los Alamos, New Mexico 87545, USA.

⁴Faculty of Biology, Technion-Israel Institute of Technology, Technion City, Haifa 3200003, Israel.

⁵Cell Signalling Research Group, School of Life Sciences, University of Nottingham, Queen's Medical Centre, Nottingham NG7 2UH, UK.

⁶Excellerate Bioscience Ltd, MediCity, Nottingham NG90 6BH, UK

*Corresponding Author. Email: michelle.halls@monash.edu

One-sentence summary: Ultra-low concentrations of ligand stimulate GPCR signaling that is distinct from that elicited by high concentrations of ligand.

Editor's Summary:

Ultra-sensitivity of GPCRs

Most analyses of signaling through G protein-coupled receptors (GPCRs) are performed using nanomolar or micromolar concentrations of ligand. Civciristov *et al.* found that femtomolar concentrations of ligand activated signaling by the endogenous β_2 adrenergic receptor (β_2 AR) and muscarinic acetylcholine receptor M₃ (M₃R) in several cell types. Such ultra-low concentrations of ligand stimulated signaling that was qualitatively distinct from that elicited by high concentrations and depended upon activation of pre-assembled GPCR complexes. In contrast, high concentrations of

ligand elicited signaling through GPCRs that were not part of complexes in addition to those in pre-assembled complexes. These findings have important implications because drugs that target GPCRs are widely used therapeutically.

Abstract

G protein-coupled receptors (GPCRs) are the largest class of cell surface signaling proteins, participate in nearly all physiological processes, and are the targets of 30% of marketed drugs. Typically, nanomolar–micromolar concentrations of ligand are used to activate GPCRs in experimental systems. We detected GPCR responses to an extraordinarily wide range of ligand concentrations, from attomolar to millimolar, by measuring GPCR-stimulated production of cyclic adenosine monophosphate (cAMP) with high spatial and temporal resolution. Mathematical modeling showed that femtomolar concentrations of ligand can activate on average 40% of cells in the population provided that a cell can be activated by one to two binding events. In addition to cAMP, activation of the endogenous β_2 adrenergic receptor (β_2 AR) and muscarinic acetylcholine M_3 receptor (M_3 R) by femtomolar concentrations of ligand in cell lines and human cardiac fibroblasts caused sustained increases in nuclear translocation of extracellular signal-regulated kinase (ERK) or cytosolic protein kinase C (PKC) activity, respectively. These responses were spatially and temporally distinct from those that occurred in response to higher concentrations of ligand and resulted in a unique cellular proteomic profile. This highly sensitive signaling depended on the GPCRs forming pre-assembled higher-order signaling complexes at the plasma membrane. Recognizing that GPCRs respond to ultra-low concentrations of neurotransmitters and hormones challenges established paradigms of drug action and provides a new dimension of GPCR activation that is quite distinct from that typically observed with higher ligand concentrations.

Introduction

G protein–coupled receptors (GPCRs) are the largest class of signaling proteins at the cell surface. These receptors can sense a diverse range of stimuli – from photons and odors to hormones and large peptides – to induce intracellular signal transduction cascades that mediate specific cellular responses. GPCRs are ubiquitously distributed across all cell types, are involved in many diseases, and are the targets of 50% of marketed drugs (1). The intracellular domains of GPCRs interact with heterotrimeric G proteins, and agonist binding to GPCRs stabilizes an active receptor conformation that promotes the dissociation of the heterotrimeric G proteins into G α and G $\beta\gamma$ subunits. The activated G proteins then interact with other intracellular effectors to induce downstream signaling. One of the downstream targets of activated G α subunits is adenylyl cyclase (AC), which converts adenosine triphosphate (ATP) into cyclic adenosine monophosphate (cAMP). However, it is increasingly clear that GPCRs do not exist in isolation. Instead, GPCR activity is closely coordinated by the assembly of receptors into higher-order protein complexes (e.g. (2-8)) that can restrict GPCR signaling to highly organized compartments within the cell, to activate receptor- and location-specific responses (2, 4, 9, 10). The spatial and temporal properties of these intracellular signals are very important for the control of distinct physiological outcomes (2, 4, 9-17).

Although the assembly of GPCRs into protein complexes enables precise spatiotemporal control over signaling, the physical interactions between the receptor and other proteins in the complex are likely to alter the pharmacological properties of the GPCR itself. We previously reported that the relaxin receptor, RXFP1, pre-assembles into a large signaling complex that facilitates activation of the receptor by attomolar concentrations of relaxin (8). Whereas responses to such “ultra-low” concentrations of biologically active compounds are well-documented in cytokine signaling (18), such high ligand sensitivity for GPCRs is not widely reported. Typically, nanomolar–micromolar concentrations of ligand are used to activate GPCRs in experimental systems using global cellular measurements, such as

calcium mobilization or cAMP accumulation assays, as readouts for GPCR activity. Nevertheless, there are reports that some GPCRs, including the β_2 -adrenergic receptor (β_2 AR), opioid receptors, and angiotensin receptors, can respond to femtomolar (10^{-15} M) concentrations of ligand in endogenous, physiological systems (19-26). Despite these observations, there is little mechanistic insight to explain these non-conventional responses, which are typically measured as changes in cell biology that occur far downstream of the receptor (such as cell adhesion or glucose uptake for the β_2 AR, analgesia or neuroprotection for opioid receptors, and blood vessel contraction for angiotensin receptors), because ultra-low ligand concentrations induce the same cellular responses or a subset of the responses as higher ligand concentrations. Without a detailed characterization of the putative extreme sensitivity of these important and ubiquitous receptors, it is unclear if this sensitivity is a widespread fundamental property of GPCRs and if ultra-low concentrations of ligands have a unique and physiologically relevant role in the cell.

Here, by measuring endogenous GPCR activity with high spatial and temporal resolution, we detected responses from various GPCRs across an extraordinarily wide range of ligand concentrations from attomolar to millimolar. We found that two prototypical GPCRs, the β_2 AR and the muscarinic acetylcholine receptor M_3 (M_3 R), were activated by femtomolar concentrations of ligand. Mathematical modeling predicted that femtomolar concentrations of ligand can feasibly activate on average 40% of cells in a population over a period of 5 min, as observed in our assays, provided that individual cells are capable of responding to 1–2 binding events. Signaling in response to femtomolar concentrations of ligand depended on the pre-assembly of a higher-order signaling complex at the plasma membrane. Compared to higher concentrations of ligand, receptor activation by femtomolar concentrations resulted in both a spatially and temporally distinct intracellular signal as well as a distinct response at the cellular level. The physical interaction between the GPCR and other proteins in the signaling complex

appeared to allosterically alter the pharmacological properties of the receptor to enhance the sensitivity to ligand. The ability of many prototypical GPCRs to respond to ultra-low concentrations of ligand suggests that a better understanding of this sensitivity is necessary for future research and drug discovery.

Results

Ultra-low concentrations of ligand activate endogenous GPCRs

Typically, GPCR ligands within the nanomolar–micromolar concentration range are reported to activate receptors in experimental systems; however, there have been reports of GPCRs responding to femtomolar concentrations of ligand, which is well below conventionally defined pEC₅₀ values, in endogenous physiological systems (e.g. (19-26)). We have previously shown that RXFP1 induces a biphasic increase in intracellular cAMP that is characterized by a remarkably wide range of pEC₅₀ values (10.9 aM vs. 0.3 nM) (8). This differs from typical biphasic response profiles, wherein each pEC₅₀ value is closely clustered within the nanomolar–micromolar concentration range (27). To determine if this sensitivity to femtomolar (and lower) concentrations of ligand is a widespread property of GPCRs, we measured cAMP following activation of members of eight different GPCR families, six of which are present endogenously in HEK293 cells and, as negative controls, two for which we could not detect any mRNA (Fig. 1, A to C and fig. S1, A to H) (28, 29). HEK293 cells endogenously produce mRNA for the A_{2B} adenosine receptor (activated by adenosine), the β₁AR and β₂AR (activated by isoproterenol, Iso) and α-adrenergic 2B and 2C sub-types, the EP₁₋₄ prostanoid receptors (activated by prostaglandin E₁, PGE₁), the M₃R (activated by carbachol, CCh), the delta opioid receptor (DOP, activated by SNC80) and the dopamine receptors, D₂R and D₄R (activated by dopamine). We found no transcripts encoding any of the receptors for relaxin (RXFP1-4) or the receptors for glucagon-like peptide 1 (GLP-1, GLP-2). The endogenous receptors canonically couple to

$G\alpha_s$ (adenosine A_{2B} , β_1AR , β_2AR , the prostanoid, relaxin and glucagon-like peptide receptors) to stimulate AC activity, $G\alpha_{i/o}$ ($\alpha_{2B}-AR$, $\alpha_{2C}-AR$, DOP, D_2R , and D_4R) to inhibit AC activity, or $G\alpha_{q/11}$ (M_3R) to stimulate Ca^{2+} mobilisation. Sub-nanomolar concentrations of adenosine, Iso, PGE_1 (Fig. 1A), CCh, SNC80, or dopamine (Fig. 1B) increased cAMP. As expected, there was no change in baseline cAMP in response to relaxin or glucagon-like peptide 1, both of which activate receptors that are not produced in HEK293 cells (Fig. 1C). For the endogenous receptors, we observed biphasic concentration-response curves ranging from attomolar to millimolar, in which the two response phases were separated by a very wide concentration range. All ligands caused an increase in cAMP at femtomolar concentrations (Table S1); when the ligand reached nanomolar concentrations, ligands that activated $G\alpha_s$ -coupled GPCRs caused a further increase in cAMP (Fig. 1A), whereas ligands that activated $G\alpha_{i/o}$ - or $G\alpha_{q/11}$ -coupled GPCRs decreased cAMP back to baseline (Fig. 1B). To determine if this characteristic biphasic response was cell type-specific, and as a further control, we repeated the same experiment in CHO-K1 cells. These cells do not endogenously produce adrenergic or muscarinic receptors (NCBI Gene Expression Omnibus accession GSE75521; (30)), and accordingly we observed no change in cAMP from baseline upon activation with Iso or CCh over a wide range of concentrations (fig. S2A). In contrast, we detected changes in cAMP following activation of members of four GPCR families that are produced endogenously (NCBI Gene Expression Omnibus accession GSE75521; (30)) in CHO-K1 cells (Fig. 1, D and E): the adenosine (A_{2A} and A_{2B}), prostanoid (EP_1 and EP_4), 5-hydroxytryptamine (5-HT; 5-HT_{1B}, 5-HT₆, 5-HT₇), and proteinase-activated (PAR1 and PAR2) receptors. Again, all ligands caused a biphasic change in cAMP from baseline: an initial increase in cAMP at femtomolar concentrations, followed by a further increase (adenosine, PGE_1 ; Fig. 1D) or a decrease back to baseline (5-HT, thrombin; Fig. 1E) when the ligand reached nanomolar concentrations. These data suggest that sensitivity to ultra-low concentrations of ligand is a potentially

fundamental property of many endogenous GPCRs, irrespective of cell type and canonical G protein–coupling profile.

To further understand this highly sensitive signaling, we selected two prototypical GPCRs for detailed examination: the β_2 AR, a classical $G\alpha_s$ -coupled receptor that responds to Iso, and the M_3 R, a classical $G\alpha_{q/11}$ -coupled receptor that responds to CCh. To our knowledge, there are no reports of muscarinic receptors responding to femtomolar concentrations of ligand; however, there are previous reports that activation of the β_2 AR by picomolar concentrations of ligand (well below the EC_{50} values) leads to increased cell adhesion (19) and glucose uptake (20). Transcripts encoding both the β_2 AR and M_3 R are endogenously produced in HEK293 cells (fig. S1, C and E), and we confirmed localization of both proteins to the plasma membrane of HEK293 cells using fluorescent ligand binding (fig. S2, B and C). Sub-nanomolar concentrations of the endogenous β_2 AR or M_3 R ligands adrenaline or noradrenaline and acetylcholine, respectively, elicited similar increases in cAMP in HEK293 cells as did the synthetic ligands Iso and CCh (Fig. 1F). We observed the same biphasic response following addition of the β_2 AR-selective agonists salbutamol and formoterol (fig. S2D); no selective M_3 R agonists are available. Further, similar highly sensitive responses to Iso and CCh were observed in primary cultures of human cardiac fibroblasts that endogenously produce β_2 AR and M_3 R (Fig. 1G and fig. S2E). This highlights that activation of endogenous GPCRs by ultra-low concentrations of ligand is a general feature of at least some endogenous systems. To confirm that responses to ultra-low concentrations of ligand were receptor-dependent, we knocked down the endogenous β_2 AR or M_3 R in HEK293 cells; this abolished cAMP responses to sub-nanomolar concentrations of Iso or CCh, respectively (Fig. 1, H to K). Knockdown of β_2 AR had no effect on the cAMP response to CCh, and knockdown of M_3 R had no effect on the cAMP response to Iso (fig. S2, F and G). This confirms that receptor knockdown did not merely reduce baseline cAMP so that responses to sub-nanomolar Iso or CCh were undetectable, but

that cAMP responses to ultra-low concentrations of Iso or CCh required β_2 AR or M_3 R, respectively. Because responses to sub-nanomolar concentrations of ligand were undetectable by the cAMP assay following exogenous expression of the β_2 AR or M_3 R (Fig. 1L), we suggest that receptor overexpression may mask the responses to sub-nanomolar concentrations of ligand typically observed in endogenous systems. This could be because overexpressed receptors cause increased constitutive activity and therefore increase the baseline cAMP concentration within the cell (compare vehicle responses in Fig. 1, A and B to Fig. 1L). Alternatively, the overexpressed receptors may alter the composition of the signaling complexes that are required to respond to ultra-low concentrations of ligand (31), thus allowing the prototypical signaling response to dominate.

We next wanted to determine whether ultra-low and high concentrations of ligand activated qualitatively different signaling pathways or only a quantitative difference in signaling. To address this we employed a sensitive plasma membrane-targeted cAMP Förster resonance energy transfer (FRET) biosensor (32) that allowed us to gain a higher resolution measure of cAMP produced at the plasma membrane in real time and in single live HEK293 cells. Activation of the endogenous β_2 AR by 1 fM Iso caused a relatively slow, gradual increase of cAMP at the plasma membrane (1.898 min^{-1}) over 5 min (Fig. 2, A and B). In contrast, a high concentration of Iso (100 nM) caused a more rapid increase in cAMP at the plasma membrane (0.666 min^{-1} , 3-fold faster than responses to 1 fM Iso), which then declined (Fig. 2, A and B). Pre-incubation of the cells with 100 nM of ICI-118,551, an adrenergic receptor antagonist, blocked the sustained plasma membrane cAMP response to 1 fM Iso (Fig. 2C and fig. S2H), further demonstrating the receptor-dependence of this signal. Whereas activation of the endogenous M_3 R by 1 fM CCh also caused a relatively slow, gradual increase in plasma membrane-associated cAMP over 5 min, there was no response to a high concentration of CCh (1 μ M; Fig. 2, D and E). The absence of a cAMP signal in response to a high concentration of CCh and the distinct

temporal profiles of cAMP generated by ultra-low vs high concentrations of Iso demonstrate that the signaling outcomes of high vs ultra-low concentrations are qualitatively different, and not merely due to changes in the amount of signaling (33). Pre-incubation of the cells with 10 nM N-methylscopolamine (NMS, a muscarinic receptor antagonist) blocked the sustained plasma membrane cAMP response to 1 fM CCh (Fig. 2F and fig. S2H), confirming the receptor-dependence of this signal. Inhibiting $G\alpha_{i/o}$ proteins with NF023 had no effect on the cAMP response to Iso or CCh (fig. S2, I and J), suggesting that differences in signaling at high concentrations are not due to the activation of additional G proteins that inhibit cAMP production. Thus, endogenous β_2 AR and M_3 R induce sustained increases in cAMP at the plasma membrane in response to remarkably low concentrations of ligand. Critically, stimulating either the ultra-low or high concentration phases resulted in different temporal signaling profiles.

Activation of GPCRs by femtomolar concentrations of ligand requires an intact orthosteric binding site

In addition to the primary orthosteric binding site, many GPCRs have allosteric binding sites within the extracellular vestibule (a surface exposed area above the binding pocket), which can fine-tune receptor activity (34). All-atom molecular dynamic simulations have demonstrated that β_2 AR and M_3 R ligands make initial contact with this extracellular vestibule prior to achieving the final pose in the orthosteric binding pocket (35, 36). We therefore wondered whether this highly responsive state of the β_2 AR and M_3 R was due to ligand binding to an allosteric, high affinity binding site, or alternatively, to the canonical orthosteric site.

In cAMP assays, the response to femtomolar concentrations of ligand was masked when the receptors were exogenously expressed (Fig. 1L). However, the plasma membrane-localized cAMP FRET

biosensor is more sensitive than the cAMP accumulation assay and has high spatial resolution, which allowed us to detect changes in cAMP abundance in single HEK293 cells in response to activation of exogenously expressed receptors by femtomolar concentrations of ligand (fig. S3, A to D). We used this approach to measure cAMP at the plasma membrane of single cells following transient expression of receptors bearing mutations in the orthosteric binding site. Mutation to alanine of a conserved orthosteric binding site residue within transmembrane domain three (D3.32A using Ballesteros-Weinstein numbering (37), essential for ligand binding to aminergic receptors (38, 39)) of β_2 AR (D113A) and M_3 R (D148A) abolished plasma membrane cAMP in response to 1 fM or 1 pM ligand (Fig. 2, G and H and fig. S4, A to D). This mutation also inhibited canonical signaling in response to high concentrations of Iso and CCh (fig. S4, A and D). To confirm that the orthosteric site was necessary for responses to ultra-low ligand concentrations, we used a well-characterized mutant form of M_3 R called M_3 R-DREADD (M_3 R designer receptor exclusively activated by designer drugs), which is selectively activated by clozapine-N-oxide (CNO) but not other ligands (40, 41) (fig. S4E). Following expression of M_3 R-DREADD in cells, 1 fM CNO, but not CCh, increased plasma membrane cAMP (Fig. 2I and fig. S4E). Taken together, this confirms that activation of β_2 AR, M_3 R, and M_3 R-DREADD by sub-nanomolar concentrations of ligand requires an intact orthosteric binding site.

Mathematical modeling supports GPCR responses to femtomolar concentrations of ligand

Cellular responses to such ultra-low concentrations of GPCR ligands are not commonly reported.

However, we have clearly shown that these responses can occur in different cell lines, are observed using distinct cell assays, are receptor-dependent, and can be eliminated by mutation of the orthosteric binding pocket. To further explore the biophysics of receptor activation at such ultra-low ligand concentrations, we developed a mathematical model based on chemical kinetics and used it to

determine whether or not the observed cell activation by ultra-low concentrations of ligands can be explained by a simple ligand-receptor interaction.

We considered a model wherein the activation of a cell is proportional to the number of occupied receptors. We also took into account the fraction of cells in the population that are competent to be activated by ligand (71.1%, determined from single cell FRET experiments using the high concentration of Iso; Fig. 2J). To simulate stochastic ligand-receptor binding kinetics in response to 1 fM Iso we used Gillespie's algorithm (42). We used a Markov chain Monte Carlo algorithm (MCMC) to sample potential parameter sets and used Bayesian statistics to estimate the probability distributions of the following parameters in our model: k_r and k_{act} (dissociation and activation rate constants, respectively), K_D (equilibrium dissociation constant), and f_c (fraction of cells competent for activation) (see Materials and Methods for model details; fig. S5, A to C). A detailed description of our procedure can be found in (43). MCMC sampling allowed us to calculate credible intervals for the time course of ligand binding in response to 1 fM Iso (Fig. 2K) and the number of binding events per cell (Fig. 2L). From this procedure, we determined the maximum *a posteriori* probability (MAP) parameter estimates (analogous to best-fit parameter estimates from non-linear regression). For the MAP parameter estimates, we found that over 70% of the cell population had less than two binding events, and less than 10% had more than two binding events in the allotted time (Fig. 2L). The average number of binding events was slightly more than one per cell. Our model therefore suggests that it is feasible for cells to respond to femtomolar concentrations of ligand, but also predicts that the cells must be sufficiently sensitive (meaning that k_{act} must be sufficiently large) to respond to just one or two binding events per cell. Such highly efficient and amplified signaling is commonly observed in response to cytokines (18). We then input the fastest published on-rate constant ($1.2 \times 10^{10} \text{ M}^{-1} \text{ min}^{-1}$ for the μ -opioid receptor ligand carfentanil) and slowest published off-rate constant ($4.8 \times 10^{-4} \text{ min}^{-1}$ for the M_3R ligand tiotropium) for a GPCR ligand (44) to evaluate the capabilities of a "super ligand". The model revealed that one binding

event per cell would occur in response to concentrations of the super ligand as low as 25 aM (attomolar, 10^{-18} M).

Responses to femtomolar concentrations of ligand depend on a pre-assembled signaling complex

We hypothesized that the signal amplification required to cause cell activation in response to 1–2 ligand binding events per cell may be achieved by the formation of highly specialized signaling complexes to allow rapid and more efficient coupling to intracellular pathways. We therefore sought to identify the signaling proteins involved in the cAMP response to femtomolar concentrations of Iso. The plasma membrane cAMP response was abolished following pharmacological inhibition of $G\alpha_s$ with NF449, of $G\beta\gamma$ with the peptide mSIRK, or of AC with 2',5'-dideoxyadenosine (ddA), suggesting that femtomolar concentrations of Iso lead to activation of AC through $G\alpha_s$ and $G\beta\gamma$ to increase plasma membrane-associated cAMP (Fig. 3A and fig. S6, A and B). Consistent with our hypothesis, complexes formed by the β_2 AR and large scaffolding proteins such as A kinase anchoring protein 79 (AKAP79), AKAP250, phosphodiesterases (PDEs), and β -arrestins are important for many responses to nanomolar concentrations of ligand (3, 5, 6). We found that the plasma membrane cAMP response to femtomolar concentrations of Iso depended on the scaffolding proteins AKAP250 and β -arrestins (Fig. 3A and fig. S6, C to F).

The plateau in the cAMP response to ultra-low ligand concentrations (Fig. 1, A, B and D to G) indicates that the balance between production and breakdown of the second messenger is tightly controlled. Whereas the proteins that are required for increased cAMP in response to activation of endogenous receptors are readily identified using inhibitors or genetic targeting, complications may arise when using the same approach to reveal proteins important for cAMP breakdown because any observed increase in basal cAMP activity could be due to the inhibitors affecting any of the multiple

endogenous receptor systems. However, by performing experiments in parallel in cells transiently expressing the β_2 AR, we can be more confident that any observed changes in baseline cAMP are due to a specific effect of the inhibitor on β_2 AR activity. The efficacy of this approach is illustrated by the identification of distinct proteins involved in the regulation of β_2 AR vs. M_3 R basal activity.

Because the β_2 AR can also couple to inhibitory $G\alpha_{i/o}$ proteins, we first assessed the effect of the $G\alpha_{i/o}$ antagonist, NF023. Inhibition of $G\alpha_{i/o}$ increased vehicle-stimulated plasma membrane cAMP in native HEK293 cells (Fig. 3B and fig. S6G) and in HEK293 cells transiently expressing the β_2 AR (Fig. 3C and fig. S6H). The same effect was observed following ADP ribosylation of $G\alpha_{i/o}$ proteins by pertussis toxin (PTx; fig. S6, I and J). This suggests there is constitutive activity of the endogenous β_2 AR in these cells which is normally tonically opposed by the activity of $G\alpha_{i/o}$. There was no additional increase in plasma membrane cAMP following stimulation with 1 fM Iso, suggesting that there is an upper limit for the induction of cAMP by the putative pre-assembled β_2 AR complex. Because cAMP can only be degraded by PDE activity, we next examined the effect of a PDE inhibitor, IBMX (3-isobutyl-1-methylxanthine). In cells both endogenously (Fig. 3B and fig. S6K) and exogenously expressing the β_2 AR (Fig. 3C and fig. S6L), IBMX pre-treatment increased vehicle-stimulated plasma membrane cAMP, with no additional increase following stimulation with 1 fM Iso. We observed the same increase in constitutive plasma membrane cAMP activity following pharmacological inhibition of protein kinase A (PKA), which is activated by cAMP and often controls feedback inhibition pathways, with KT5720 (Fig. 3, B and C and fig. S6, K and L). PDE4D contributes a high proportion of PDE activity in HEK293 cells (45), and PKA activates the long isoforms PDE4D3 and PDE4D5 (46). Over-expression of dominant negative (dn) forms of PDE4D3 (PDE4D3 dn) and PDE4D5 (PDE4D5 dn) caused an increase in vehicle-stimulated plasma membrane cAMP in native HEK293 cells (Fig. 3B and fig. S6, M and N). Whereas 1 fM Iso stimulated an additional increase in plasma membrane cAMP in

cells expressing PDE4D3 dn, there was no further increase compared to vehicle in cells expressing PDE4D5 dn. This suggested that although PDE4D5 may repress the constitutive activity of the putative pre-assembled β_2 AR complex, PDE4D3 merely decreases basal cAMP globally in the cell. Indeed, when we performed the same experiment in cells transiently expressing the β_2 AR, only co-expression of PDE4D5 dn, but not PDE4D3 dn, caused the same increase in vehicle-stimulated plasma membrane cAMP with no further increase in response to 1 fM Iso (Fig. 3C and fig. S6O). Because PKA is tethered in close proximity to the β_2 AR under resting conditions by the scaffolding protein AKAP79 (3), we assessed the effect of AKAP79 knockdown on cAMP production. Knockdown of AKAP79 (fig. S6P) significantly increased vehicle-stimulated plasma membrane cAMP, and there was no further increase in plasma membrane cAMP following the addition of 1 fM Iso in native HEK293 cells (Fig. 3B and fig. S6Q) and or in cells exogenously expressing the β_2 AR (Fig. 3C and fig. S6R). This suggests that AKAP79 plays an important role in repressing responses to 1 fM Iso.

That the inhibition of proteins that repress cAMP production causes an increase in signaling under non-stimulated conditions (Fig. 3, B and C) suggests both an inherent constitutive activity of the β_2 AR signaling complex, and that it may be pre-assembled under non-stimulated conditions. To confirm this, and to also identify the region of the receptor that interacts with other proteins in the complex, we performed glutathione S-transferase (GST) pulldowns using the intracellular regions of the β_2 AR (Fig. 3D and fig. S7A). Under non-stimulated conditions, proteins required for activation ($G\alpha_s$, AC2, β -arrestin 1 and 2) and inhibition ($G\alpha_i$, PKA, PDE4D5 and AKAP79) of the β_2 AR interacted with C-terminal helix 8 (CT1, residues 330-357) (Fig. 3, E to G and fig. S7, A to D). Although we could not readily detect interactions with some proteins encoded by transcripts that occur at very low abundance in HEK293 cells (AC, AKAP79, and PDE4D; fig. S7E), exogenous expression of the protein of interest enabled detection of interactions with GST-CT1. This also revealed the involvement of AC2 in the

production of cAMP downstream of β_2 AR: $G\alpha_s$ and $G\beta\gamma$ coincidentally activate AC2, AC4, and AC7 (47), and β_2 AR GST-CT1 pulled down exogenously expressed AC2-HA from cell lysates. Further, although we were unable to pull down $G\alpha_i$ from native HEK293 cell lysates, β_2 AR GST-CT1 pulled down endogenous $G\alpha_i$ from HEK293 cell lysates transiently expressing AC2-HA, PDE4D5 dn, or AKAP79-HA (Fig. 3, F and G and fig S7B). The propensity of AKAP250 to oligomerize (48) prevented pulldown of endogenous or exogenously expressed AKAP250, however, exogenously expressed HA-AKAP250 coimmunoprecipitated with the endogenous β_2 AR under non-stimulated conditions (Fig. 3H). To confirm that the β_2 AR signaling complex was pre-assembled at the plasma membrane in intact cells, we used acceptor photobleaching FRET to monitor interactions between cyan fluorescent protein (CFP)-tagged β_2 AR (β_2 AR-CFP) and some yellow fluorescent protein (YFP)-tagged components of the complex ($G\alpha_s$, AKAP79, β -arrestins 1 and 2, PKA) identified in signaling and GST pulldown experiments (Fig. 3I). We measured FRET within two regions of the plasma membrane for each cell analysed. Despite colocalization of proteins, FRET was not always detected in both regions of the plasma membrane (Table S2), suggesting the β_2 AR signaling complex is only formed in discrete membrane domains. Due to this non-uniform formation of the β_2 AR signaling complex, the data is not normally distributed. Analysis of the FRET efficiency revealed significant interactions at the plasma membrane under basal conditions between β_2 AR-CFP and $G\alpha_s$ -YFP and PKA-YFP, versus the negative control $G\alpha_q$ -YFP (Fig. 3J). Conversion of the data to binary values (0 = no FRET, 1 = FRET) revealed significant FRET between β_2 AR-CFP and all components tested: $G\alpha_s$ -YFP, AKAP79-YFP, YFP- β -arrestin1, YFP- β -arrestin2, and PKA-YFP (Fig. 3J and fig. S7F). Therefore, a pre-assembled β_2 AR signaling complex responded to 1 fM Iso by stimulating $G\alpha_s$ - $G\beta\gamma$ activation of AC2 to increase cAMP in a manner that depended on AKAP250 and β -arrestins. This

cAMP production was tonically opposed by $G\alpha_{i/o}$ inhibition of AC2, and PKA stimulated PDE4D5 activity in a manner that depended on AKAP79 (Fig. 3K).

The cAMP produced in response to activation of the M_3R by 1 fM CCh required a set of proteins distinct from those required for cAMP production downstream of the β_2AR . There was no effect of $G\alpha_s$ inhibition on the plasma membrane cAMP response to 1 fM CCh (Fig. 4A and fig. S8A), suggesting that an alternate pathway can activate AC in this context. Activation of the M_3R by micromolar concentrations of CCh induces a cAMP response that depends on a signaling complex comprising AKAP79, AC2, PKC, PKA, and $G\alpha_{q/11}$ (7). Similarly, we found that the plasma membrane cAMP response to femtomolar concentrations of CCh was abolished following pharmacological inhibition of $G\alpha_{q/11}$, $G\beta\gamma$, PKC, and AC (Fig. 4A and fig. S8, A to C). Thus, for the M_3R , ultra-low concentrations of ligand lead to $G\alpha_{q/11}$ - $G\beta\gamma$ activation of PKC, which stimulates AC to increase cAMP. In contrast to the β_2AR complex, there was no effect of knockdown of AKAP250; however, knockdown of either β -arrestin 1 or β -arrestin 2 abolished the plasma membrane cAMP response to 1 fM CCh (Fig. 4A and fig. S8, D to E).

As observed for the β_2AR (Fig. 3, B and C), inhibition of $G\alpha_{i/o}$ increased vehicle-stimulated plasma membrane cAMP in native HEK293 cells; however, 1 fM CCh stimulated a further increase in plasma membrane cAMP compared to the vehicle control (Fig. 4B and fig. S8F). This suggests that $G\alpha_{i/o}$ does not inhibit the pre-assembled M_3R signaling complex. Indeed, in HEK293 cells transiently expressing the M_3R there was no effect of the $G\alpha_{i/o}$ antagonist NF023 on the plasma membrane cAMP produced in response to vehicle or 1 fM CCh (Fig. 4C and fig. S8G). The same effect was observed following ADP ribosylation of $G\alpha_{i/o}$ proteins by PTx (fig. S8, H and I). In contrast, inhibition of PDEs or PKA increased vehicle-stimulated plasma membrane cAMP in both native HEK293 cells (Fig. 4B and fig.

S8J) and following transient expression of the M₃R (Fig. 4C and fig. S8K), with no further increase in plasma membrane cAMP following stimulation with 1 fM CCh. This confirmed that the M₃R also displays an inherent constitutive activity that is likely due to pre-assembly of a signaling complex, as identified for the β_2 AR. Expression of both PDE4D3 dn and PDE4D5 dn in native HEK293 cells caused a significant increase in vehicle-stimulated plasma membrane cAMP, with no further increase in plasma membrane cAMP in response to 1 fM CCh (Fig. 4B and fig. S8L). However, following co-expression of the M₃R, only PDE4D3 dn caused an increase in vehicle-treated plasma membrane cAMP with no further increase in response to 1 fM CCh (Fig. 4C and fig. S8M). Therefore, as for responses to high concentrations of CCh (7), PDE4D3 represses cAMP activity of the M₃R. AKAP79 was required for negative regulation of the β_2 AR complex. Although knockdown of AKAP79 increased vehicle-stimulated plasma membrane cAMP in native HEK293 cells (Fig. 4B and fig. S8N), it did not affect plasma membrane cAMP in response to vehicle treatment but did abolish the response to 1 fM CCh in cells transiently co-expressing the M₃R (Fig. 4C and fig. S8O). Thus, as for cAMP responses to micromolar concentrations of CCh (7), an increase in cAMP in response to 1 fM CCh depended on AKAP79.

To confirm that these proteins can pre-assemble with the M₃R, we performed GST pulldowns from unstimulated HEK293 cell lysates and showed that proteins required for activation ($G\alpha_{q/11}$, PKC, AC2, β -arrestins 1 and 2, AKAP79) and repression (PKA, PDE4D3) of ultra-sensitive M₃R signaling required residues 305-457 of the third intracellular loop (ICL3) of M₃R for assembly into a complex with the receptor (Fig. 4, D to G and fig. S9, A to D). As we observed with the β_2 AR, we could not detect endogenous interactions with some proteins encoded by transcripts that occurred at very low abundance in HEK293 cells (AC, AKAP79, and PDE4D; fig. S7E), but exogenous expression of the protein of interest enabled detection of interactions between these proteins and the GST-tagged regions

of M₃R (Fig. 4, D to G and fig. S9, A to D). Again, as with β_2 AR, this also revealed the involvement of AC2 in the stimulation of cAMP downstream of M₃R. PKC and G $\beta\gamma$ can activate AC2 (47), and M₃R GST-ICL3-2 pulled down exogenously expressed AC2-HA from cell lysates. We were unable to pull down PKC from native HEK293 cell lysates; however, endogenous PKC was pulled down by GST-ICL3-2 from cell lysates transiently expressing AC2-HA, AKAP79-HA, or PDE4D3 dn (Fig. 4, D and G). As with the β_2 AR, to confirm pre-assembly of the M₃R signaling complex at the plasma membrane of intact cells, we used acceptor photobleaching FRET between M₃R-CFP and YFP-tagged components (G α_q , AKAP79, β -arrestins 1 and 2, PKA and PKC) of the signaling complex (Fig. 4H). Formation of the M₃R complex did not always occur in regions of protein co-localization (Table S2), and the data was non-normally distributed, suggesting the M₃R signaling complex forms in discrete regions of the plasma membrane. Analysis of the FRET efficiency revealed significant interactions between M₃R-CFP and G α_q -YFP, YFP- β -arrestins 1 and 2, and YFP-PKC, versus the negative control G α_s -YFP (Fig. 4I). Following conversion of the data to binary values (0 = no FRET, 1 = FRET), we observed significant FRET between the M₃R-CFP and all components tested: G α_q -YFP, AKAP79-YFP, YFP- β -arrestin1, YFP- β -arrestin2, PKA-YFP, and YFP-PKC (fig. S9E). Therefore, a pre-assembled M₃R signaling complex responds to 1 fM CCh by stimulating G $\alpha_{q/11}$ -G $\beta\gamma$ -PKC-mediated activation of AC2 to increase cAMP in a manner that depends on AKAP79 and β -arrestins, and this cAMP is tonically opposed by PKA stimulated PDE4D3 (Fig. 4J).

Together, these data reveal that although activation of the β_2 AR and M₃R by femtomolar concentrations of ligand produces the same sustained increase in cAMP, the responses require pre-assembly of signaling complexes comprising a distinct subset of proteins that associate with different regions of the receptors (Fig. 3K and 4J).

GPCRs activate sustained, compartmentalized signals in response to femtomolar concentrations of ligand

Next we investigated if signaling in response to femtomolar concentrations of ligand extends to downstream pathways other than cAMP, if this signaling differs from that induced by high concentrations of ligand, and if this also occurs in human cardiac fibroblasts. We measured changes in ERK and PKC activity in different sub-cellular domains using FRET biosensors (that contain phosphorylation target sequences for ERK or PKC, respectively) targeted to different areas of the cell (49-51). Activation of the endogenous β_2 AR in HEK293 cells and human cardiac fibroblasts did not affect the activity of cytosolic ERK, but increased nuclear ERK activity in individual cells (Fig. 5, A to D and fig. S10A). Mimicking the temporal dynamics of the cAMP response (Fig. 5, E and F), 1 fM Iso caused a sustained increase in nuclear ERK, whereas 100 nM Iso resulted in a transient increase (Fig. 5, A and D). There was no effect of 1 fM CCh on ERK activity in HEK293 cells (Fig. 5C) or in the cardiac fibroblasts (fig. S10B). In contrast, 1 fM CCh caused a sustained increase in cytosolic, but not plasma membrane-localized, PKC activity in both cell types (Fig. 5, G to J and fig. S10C); whereas a high concentration (1 μ M) generated a transient increase in cytosolic PKC activity in both cell types and an increase in plasma membrane PKC activity in the cardiac fibroblasts (Fig. 5, G to J and fig. S10C). This again mimicked the temporal dynamics of the M_3 R cAMP response: 1 fM CCh caused a sustained increase in plasma membrane-localized cAMP, whereas 1 μ M CCh induced a delayed and transient increase in plasma membrane cAMP that peaked at 15 min in HEK293 cells and at 5 min in the cardiac fibroblasts (Fig. 5, K and L). There was no effect of 1 fM Iso on PKC activity in the two cell types (Fig. 5I and fig. S10D). Therefore, activation of GPCRs by ultra-low concentrations of ligand also affects other intracellular signaling pathways in addition to cAMP production. In contrast to responses to high concentrations of ligand, this signaling is sustained and restricted to defined sub-cellular compartments. This demonstrates that activation of GPCRs by ultra-low concentrations of

ligand induces signaling that is qualitatively different compared to the canonical responses activated by concentrations in the nanomolar to micromolar range.

Activation of GPCRs by femtomolar concentrations of ligand causes a unique cellular response

Both the location and duration of intracellular signals are extremely important for generating appropriate and distinct cellular responses (2, 4, 9). Because GPCR activation by femtomolar concentrations of ligand causes sustained signals in defined cellular compartments, this suggests that each femtomolar GPCR response may orchestrate a distinct cellular signal compared to both higher ligand concentrations and other ligands at femtomolar concentrations. Here we employed proteomic analysis by liquid chromatography coupled to tandem mass spectrometry (LC-MS/MS) as a sensitive and global assessment of the consequences of activation of endogenous GPCRs by femtomolar concentrations of ligand in HEK293 cells. Activation of endogenous GPCRs induced a proteomic pattern that was unique to both the receptor that was stimulated and the ligand concentration (Fig. 6, A and B and Table S3). For the β_2 AR, the abundances of 56 proteins were uniquely affected by 1 fM Iso compared to vehicle or 100 nM Iso. From these, we identified proteins that were exclusively increased in response to 1 fM Iso, but not in response to 100 nM Iso or either concentration of CCh. These included five proteins that have roles in RNA processing and protein synthesis (Fig. 6C): SF3B5 (splicing factor 3B subunit 5), a component of the spliceosome important for pre-mRNA splicing; TXNL4A (thioredoxin-like protein 4A), part of the machinery involved in spliceosome assembly; RPS21 (40S ribosomal protein 21), a component of the 40S ribosomal subunit; GUF1 (translation factor GUF1), promotes protein synthesis and acts as a fidelity factor during translation; and TXNDC9 (thioredoxin domain-containing protein 9), which negatively impacts protein folding by inhibiting the ATPase activity of the chaperonin TCP1 complex. These results, in addition to the sustained increase in nuclear ERK activity (Fig. 5, A to C), suggested that ultra-low concentrations of Iso may affect gene expression. In agreement with the proteomic data, only 1 fM Iso, but not 100 nM Iso or CCh, increased

gene transcription over a period of 4 hours (Fig. 6, D and E) as assessed by a GFP reporter under the control of the constitutive EF1 α promoter. We observed a similar increase in gene transcription in response to 1 fM Iso, but not 100 nM Iso or CCh, in human cardiac fibroblasts (Fig. 6, F and G). In HEK293 cells we observed no effect of inhibition of G $\alpha_{i/o}$ by NF023 on the lack of response to 100 nM Iso (fig. S10E). This shows that the absence of a signal in response to 100 nM Iso was not due to activation of inhibitory pathways and that therefore the responses to 1 fM and 100 nM Iso are qualitatively different. Together, these data demonstrate a unique role for increased gene transcription in cellular responses to the activation of the β_2 AR by femtomolar concentrations of ligand that is not triggered by higher concentrations of ligand.

Similarly for the M $_3$ R, 1 fM CCh affected the abundances of 35 proteins in HEK293 cells compared to vehicle or 10 μ M CCh. From these, we identified proteins that were exclusively increased in response to 1 fM CCh but unaffected by 10 μ M CCh or either concentration of Iso. These included five proteins that affect trafficking, cytoskeletal networks and small G protein signaling (Fig. 6H): GGA1 (ADP-ribosylation factor-binding protein), which plays a role in protein sorting and trafficking between the trans-Golgi network and endosomes; PDE6D (a cGMP PDE), which regulates the sub-cellular targeting of Ras small GTP-binding proteins; ILK (integrin-linked protein kinase), which is implicated in cell architecture, adhesion and anchorage-independent growth; VPS52 (vacuolar protein sorting-associated protein 52), which is a component of the retrograde transport and endocytic recycling machinery; and GPSM1 (G protein signaling modulator 1), a guanine nucleotide dissociation inhibitor which uncouples G protein signaling from GPCRs. These results suggested that ultra-low concentrations of CCh might be important for the regulation of cellular trafficking, cytoskeletal organization and signaling by small G proteins. To test this hypothesis we used Raichu-Cdc42, a FRET biosensor that reports on activation of the Rho GTPase Cdc42 (52); Rho GTPases are small G proteins that are important regulators of

trafficking and cytoskeletal organization (53). Indeed, in agreement with the proteomic data, over 4 hours only 1 fM CCh caused an increase in Cdc42 activity, but 10 μ M CCh, 1 fM Iso, and 100 nM Iso did not (Fig. 6, I and J). We observed the same increase in Cdc42 activity in response to 1 fM CCh, but not 10 μ M CCh or Iso, in the human cardiac fibroblasts (Fig. 6, G and K). As seen for cAMP, inhibition of $G\alpha_{i/o}$ by NF023 did not alter the lack of response to 10 μ M CCh (fig. S10F) in HEK293 cells. This shows that 10 μ M CCh did not increase Cdc42 activity and that the responses to 1 fM and 10 μ M CCh are qualitatively different. Therefore, activation of the M_3R by femtomolar concentrations of CCh causes an increase in Cdc42 activity, which can impact many basic cellular processes including cell morphology, migration, endocytosis, and cell cycle progression (49). As seen for the β_2AR , these data demonstrate that activation of the M_3R by ultra-low ligand concentrations generates a unique cellular response compared to high ligand concentrations.

Discussion

The current findings uncover a previously unappreciated dimension of GPCR signaling, with several prototypical GPCRs initiating cellular responses to sub-nanomolar concentrations of ligand that are distinct from responses elicited by higher ligand concentrations. This extremely high sensitivity of GPCRs to ligand was observed in multiple cell types, was receptor-dependent, and required an intact orthosteric binding site in the receptor. Mathematical modeling suggested that these responses were triggered in an individual cell by one to two binding events, which would necessitate signal amplification. The pre-assembled signaling complexes we identified may play an important role in amplifying the response to individual receptor binding events by allowing highly efficient coupling to the signaling machinery. Activation of GPCRs by ultra-low concentrations of ligand caused sustained signals within defined subcellular compartments. In contrast, higher concentrations of ligand enabled

many more binding events to receptors both within and outside of complexes to generate qualitatively different responses at the whole-cell level (Fig. 7).

Although a sensitivity to femtomolar concentrations of biological compounds is well below the accepted binding affinity of GPCRs, we were able to simulate stochastic ligand binding kinetics to reveal that the addition of femtomolar solutions of ligand under our assay conditions would result in, on average, roughly one binding event per cell over 5 min. This suggests firstly, that responses to ultra-low concentrations of ligand are triggered by only a few GPCR molecules at the cell surface, and secondly, that activation of one–two receptors results in highly efficient signal amplification. Such signal amplification resulting from activation of only a few receptors at the cell surface is commonly observed for cytokine receptors (18). There are several ways in which such a high degree of signal amplification could occur. Our studies using inhibitors, GST pulldowns, and acceptor photobleaching FRET suggest that a pre-assembled, functional, higher-order signaling complex is essential for responses to ultra-low concentrations of ligand, and that the inherent activity of the GPCR is tightly controlled and limited. The close proximity of receptor, G proteins, and effectors to one another would allow a small number of activated receptors to cause a very rapid increase in signaling. Moreover, an assembled signaling complex may alter the local environment of a ligand near a receptor in such a way that the ligand spends more time in close proximity to the receptor, perhaps allowing a ligand to rebind to the receptor multiple times or to bind to the receptor for a longer time, thereby increasing the apparent sensitivity of the receptor to the ligand (54, 55). Indeed, the mere presence of β_2 AR at the plasma membrane of cells can more than double the local concentration of ligand (56). In addition, if these signaling complexes cluster due to oligomerization of AKAPs (48, 57), this would result in a high local concentration of receptors at the plasma membrane, with the clustered receptors effectively acting as a “ligand sink” to again increase the apparent receptor affinity. Finally, the protein-protein interactions within the complex may allosterically alter the properties of other associated proteins. This

could conceivably result in higher affinity binding by the receptor, by locking the transmembrane helices in an open conformation or reducing the dynamic fluctuations of the ligand binding site, to increase ligand accessibility to the binding pocket or to stabilize the ligand-receptor interaction to generate a signal robust enough to elicit a cellular response. In fact, binding of a positive allosteric nanobody to the intracellular regions of the β_2 AR can increase the affinity of β_2 AR for Iso by up to 15,000-fold (58); this demonstrates that intracellular allosteric modulation of a subset of receptors could create two defined receptor populations with widely different ligand sensitivity. Allosteric interactions within the signaling complex may also lower the activation threshold of G proteins and other downstream effectors. Previous studies suggest that the association of PKC with AKAP79 locks the kinase into an active conformation, and PKC becomes insensitive to inhibitors that compete with ATP for binding to the kinase (59, 60). For the M_3 R, this heightened PKC activity could be very important for facilitating the efficient activation of AC2 by the kinase in response to ultra-low concentrations of CCh.

The production, activity, and degradation of cAMP following stimulation of both the β_2 AR and M_3 R by femtomolar concentrations of ligand involves many proteins that are also required for responses to high concentrations of ligand (3, 5-7, 61). Although high-sensitivity responses are associated with many familiar components of GPCR signaling, the dynamics of the interacting proteins within the signaling complex must differ depending on the abundance of ligand to produce unique signaling outcomes. We found that the proteins of the pre-assembled β_2 AR complex interacted with the CT1 region of the C-terminal tail of β_2 AR. This is consistent with previous reports of interactions between the C-terminal tail of the β_2 AR and proteins such as AKAP79, AKAP250, PKA, G protein receptor kinase 2 (GRK2), and Src (3, 61, 62). All proteins within the pre-assembled M_3 R complex interacted with the ICL3 domain of M_3 R. This is also consistent with previous reports of interactions between the

M₃R ICL3 and proteins such as G $\alpha_{q/11}$, G $\beta\gamma$, phospholipase C β , GRKs, β -arrestins, and casein kinase 2 (63-66). Moreover, conformational changes within this loop region are important for the formation of M₃R dimers (67). For both the β_2 AR and M₃R, a large number of proteins interact with the receptors through the same intracellular regions. However, crystal structures of the β_2 AR in complex with G α_s (68) and electron microscopy reconstruction of the β_2 AR in complex with β -arrestin (69) or a β_2 AR/V₂ vasopressin receptor chimera in complex with both G α_s and β -arrestin (70) suggest that there is little available space for any additional proteins to interact with a monomeric receptor. Nevertheless, these sorts of interactions may be feasible due to the highly flexible structure of AKAPs and the tendency for both AKAP250 and AKAP79 to form higher-order homo- and hetero-oligomeric structures (48, 57). AKAPs may therefore play an important role in supporting the efficient scaffolding of a large number of proteins. Consequently, we may envisage a higher-order assembly of a signaling complex that, by scaffolding a large number of effector proteins, generates a high amount of signal amplification in close proximity to the receptor.

Responses to very subtle environmental cues have been described from bacteria to mammals. Some metalloregulatory proteins have femtomolar sensitivity to control zinc homeostasis in bacteria (71, 72), and it is proposed that *Escherichia coli* use sub-femtomolar zinc sensing to gain information about the host niche and form biofilms only in certain environments (73). Similarly, bacteria sense host iron as an environmental cue to express virulence factors (74); free iron is kept at ultra-low levels (10 yoctomolar; 10⁻²⁴M) in vertebrates (75), so bacterial siderophore proteins bind iron with extremely high affinity (enterobactin binds iron with a K_d of 10⁻³⁵M) (76, 77). Here we show that mammalian cells can generate qualitatively unique responses to ultra-low concentrations of GPCR ligands. It is therefore tempting to speculate that the purpose of this high sensitivity is similar: to assess or sample the niche and tailor cellular phenotypes accordingly. Thus we could anticipate that cells exposed to ultra-low

concentrations of adrenaline may develop a phenotype distinct from cells that are exposed to ultra-low concentrations of acetylcholine. We suggest that this extremely large dynamic range of GPCR signaling is widespread throughout this receptor superfamily and that a low amount of continuous receptor activation may play a critical role in maintaining cell phenotypes in response to subtle environmental cues. The realization that many prototypical GPCRs respond to ultra-low concentrations of ligand has important implications for the current understanding of GPCR signaling and the drug design process. XX For example, current treatment regimens do not consider dosage to such low levels, or whether drugs can discriminate between isolated receptors or receptors assembled into protein complexes, as mechanisms for response specificity. This may go some way towards explaining the high attrition rates in GPCR drug development. Translation of these concepts could allow “repurposing” of existing drugs using tailored dosage or by targeting the drugs to specific protein complexes.

Materials and Methods

cDNAs

AC2-HA (8) and AKAP79-HA (78) were described previously. The pEF1 α -AcGFP-C1 vector was from Clontech, and human M₃R and 3HA-M₃R were from the Bloomsburg University cDNA Resource Centre (www.cdna.org). Human β_2 AR (79) was a gift from R Summers, and FLAG- β_2 AR (80) was a gift from R Lefkowitz. M₃R-DREADD (Y149C, A239G) (40) was a gift from B Roth. Dominant negative PDE4D3 D484A (81) and PDE4D5 D556A (82) were gifts from M Houslay. HA-AKAP250 (83) was a gift from C Malbon, and pSilencer and AKAP79 shRNA (59) were gifts from J Scott.

pmEpac2 (32) was a gift from D Cooper. nucEKAR EGFP-mRFP (Addgene plasmid 18682) and cytoEKAR EGFP-mRFP (Addgene plasmid 18680) were gifts from K Svoboda (49). CytoCKAR (Addgene plasmid 14870) and pmCKAR (MyrPalm-CKAR, Addgene plasmid 14862) were gifts from

A Newton (50, 51). Raichu-Cdc42 (Raichu-Cdc42/Cdc42CT) was a gift from M Matsuda (52), and was contained within the pCAGGS vector (84), which was a gift from J Miyazaki.

G α_s -YFP (Addgene plasmid 55781) and G α_q -YFP (Addgene plasmid 55782) were gifts from C Berlot (85). AKAP79-YFP (AKAP79 in a pEYFP-N1 vector) was a gift from M Dell'Acqua (86). YFP- β -arrestin 1 and YFP- β -arrestin 2 were gifts from M Caron (87). PKA catalytic subunit-YFP (PKA-YFP) was a gift from M Zaccolo (88). YFP-PKC- β II-YFP (YFP-PKC; Addgene plasmid 14866) was a gift from A Newton (50).

FLAG- β_2 AR D3.32A (D113A) and 3HA-M $_3$ R D3.32A (D148A) were generated using the Quikchange II kit (Agilent Technologies). The D3.32A annotation uses the Ballesteros-Weinstein numbering system (37). FLAG- β_2 AR-CFP and 3HA-M $_3$ R-CFP were generated by sub-cloning FLAG- β_2 AR and 3HA-M $_3$ R into pECFP-N1. GST-tagged fragments of the β_2 AR and M $_3$ R intracellular regions were generated by amplifying the required region from the full-length cDNA using PCR, and cloning into pGEX-4T1. Shorter regions (β_2 AR-ICL1, β_2 AR-ICL2, M $_3$ R-ICL1 and M $_3$ R-CT1) were generated by annealing complementary primers, and cloning into pGEX-4T1. The following GST-tagged fragments of the β_2 AR were generated: ICL1 (residues 59-71), ICL2 (134-150), ICL3 (221-274), CT (330-413), CT1 (330-357), CT2 (358-386), and CT3 (387-413). The following GST-tagged fragments of the M $_3$ R were generated: ICL1 (91-104), ICL2 (165-185), ICL3 (256-489), ICL3-1 (256-304), ICL3-2 (305-457), ICL3-3 (458-489), CT (546-590), CT1 (546-560), and CT2 (561-590).

Drugs

The vehicle for Iso, adrenaline, noradrenaline, dopamine and serotonin was 0.1% w/v ascorbic acid, present in experiments at a final concentration of 0.0001% w/v. The vehicle for CCh, adenosine,

salbutamol, acetylcholine and thrombin was ultra-pure (MilliQ) water and for CNO, PGE₁, SNC80 and formoterol was DMSO, both present in experiments at a final concentration of 0.01% v/v. The vehicle for relaxin was 0.1% v/v trifluoroacetic acid, present in experiments at a final concentration of 0.0001% v/v, and for glucagon-like peptide 1 was 0.025% v/v acetic acid, present in experiments at a final concentration of 0.000025% v/v.

Cell culture

HEK293 and CHO-K1 cells (ATCC; negative for mycoplasma contamination) were used as well-characterized generic cell lines with endogenous expression of GPCRs. The cells were grown in DMEM supplemented with 5% v/v FBS. For HEK293 cells all assay dishes and plates were pre-coated with poly-D-lysine (5 µg/cm²). Primary cultures of human cardiac fibroblasts (ScienCell) were grown in poly-L-lysine coated culture flasks (2 µg/cm²) in DMEM supplemented with 5% v/v FBS, fibroblast growth supplement 2 (ScienCell), 100 U/mL penicillin and 100 µg/mL streptomycin.

HEK293 cells were transfected using linear polyethyleneimine (PEI) (89). For experiments using single transfection of siRNA (AlphaScreen cAMP assay), cells were transfected with 25 nM scrambled, β₂AR or M₃R SMARTpool ON-TARGETplus siRNA (GE Dharmacon) using Lipofectamine 2000 (Invitrogen). Human cardiac fibroblasts were transfected using X-tremeGENE 9 (Roche) at a 1:3 DNA:transfection reagent ratio.

RNA sequencing

RNA was extracted from two passages of HEK293 cells (P0 and P37) using the RNeasy Mini Kit (Qiagen), and transcriptome sequencing was performed by the Beijing Genomics Institute.

cAMP quantification assay

cAMP from cell populations was measured in duplicate using the AlphaScreen cAMP accumulation assay (PerkinElmer) as described previously (90) with the following modifications to ensure the maximum dynamic range and sensitivity. Cells were seeded into 96-well plates and grown to confluency. On the day of the experiment, cells were pre-incubated with stimulation buffer (HBSS with 5 mM HEPES, 5.6 mM glucose, 1.3 mM CaCl₂, 0.1% w/v BSA, pH 7.4) for 45 min at 37°C, prior to addition of ligands, vehicle or positive control (50 μM forskolin, 100 μM IBMX) diluted in stimulation buffer for 30 min at 37°C. For HEK293 cells and human cardiac fibroblasts, the experiment was performed in the absence of PDE inhibition; for CHO-K1 cells, the experiment was performed in the presence of 500 μM IBMX. To terminate the reaction, buffer was aspirated and 50 μL ice-cold ethanol was added per well. Following ethanol evaporation at 37°C, the cell precipitate was resuspended in 30 μL detection buffer (5 mM HEPES, 0.3% Tween-20, 0.1% w/v BSA, pH 7.4; 130 μL for positive control samples), then 10 μL was transferred to a 384-well white OptiPlate (PerkinElmer) on ice. Following addition of anti-cAMP acceptor beads (in the presence of 500 μM IBMX) and donor beads with biotinylated cAMP for 1 h, the plate was read using an EnVision Multilabel Reader (PerkinElmer), and data analyzed against a standard curve using GraphPad Prism from *n* biological repeats as stated.

qRT-PCR

RNA was extracted from HEK293 cells and primary human cardiac fibroblasts using the RNeasy Mini Kit (Qiagen). qRT-PCR was performed in triplicate from 100 ng RNA using the iScript One-Step RT-PCR Kit (Bio-Rad) and CFX96 Real Time System (Bio-Rad) according to manufacturer's instructions. TaqMan probes (Applied Biosystems) used in this study were: *ADRB2*: Hs00240532_s1; *CHRM3*: Hs00265216_s1 and *ACTB*: Hs99999903_m1. The 2^{-ΔCT} method (91) was used to analyze results and

data are expressed as $2^{-\Delta\text{CT}}$ (difference in Ct value of the gene of interest relative to the housekeeping gene, *ACTB*) from n biological repeats as stated.

Fluorescent ligand binding

HEK293 cells were seeded into black, optically clear 96-well plates and grown to 80% confluency. Cells were washed in PBS, then incubated with a nuclear stain (Hoescht 33342, Pierce) and a saturating concentration of antagonist (1 μM ICI-118,551 for $\beta_2\text{AR}$ binding or 100 μM N-methyl scopolamine for M_3R binding) or vehicle control for 1 hour at RT. The fluorescent ligands (1 μM BODIPY-propranolol for $\beta_2\text{AR}$ binding or 100 nM BODIPY-pirenzepine for M_3R binding, both from CellAura) were added for 10 min at RT. Buffer was removed from the cells and replaced with PBS prior to fluorescence imaging using a high-content PerkinElmer Operetta with an Olympus LUCPlanFLN 20x (NA 0.45) objective. Nuclei were visualized using the Hoescht 33342 filter set (excitation 360-400, emission 410-480) and BODIPY fluorescence was visualized using the Cy5 filter set (excitation 620-640, emission 640-680). Four fields of view were captured per well and data were automatically analysed by determining the mean BODIPY fluorescence per well using Harmony High Content Imaging and Analysis software (v3.5.2). BODIPY fluorescence was expressed relative to the vehicle-treated control in triplicate from n biological repeats, as stated.

High-content ratiometric FRET imaging

Ratiometric FRET imaging was performed as described previously (9, 89, 92). We detected changes in cAMP levels using Epac2-camps (93) targeted to the plasma membrane (32) which undergoes a conformational change following cAMP binding to the cAMP-binding domain of Epac2. Changes in ERK or PKC activity were detected using EKAR or CKAR, respectively, which undergo conformational change following ERK or PKC phosphorylation of a target sequence. We used EKAR

targeted to the cytosol or nucleus (49), and CKAR targeted to the plasma membrane or cytosol (50, 51). Changes in Cdc42 activity were detected using Raichu-Cdc42 which undergoes a conformational change after GTP displaces GDP within residues 2-176 of Cdc42 (52).

HEK293 cells were seeded in black, optically clear 96-well plates and grown to 70% confluency prior to transfection with PEI. Human cardiac fibroblasts were transfected using X-tremeGENE 9 in suspension and seeded in half area black, optically clear 96-well plates at 90% confluency. To measure activation of endogenously expressed receptors, HEK293 cells were transfected with 90 ng/well FRET biosensor and human cardiac fibroblasts were transfected with 100 ng/well FRET biosensor. For over-expression of mutant receptors, HEK293 cells were co-transfected with 55 ng/well receptor and 40 ng/well FRET biosensor. For experiments with siRNA, HEK293 cells were co-transfected with an additional 25 nM scrambled, β -arrestin 1, β -arrestin 2 or AKAP250 SMARTpool ON-TARGETplus siRNA (GE Dharmacon) for 72 hr. For experiments involving dominant negative constructs or shRNA, HEK293 cells were co-transfected with an additional 50 ng/well plasmid for 72 hr. Prior to the experiment, HEK293 cells were partially serum-restricted overnight in 0.5% FBS v/v DMEM.

Cells were pre-treated with inhibitors for 30 min at 37°C in HBSS and inhibitors were used at the following concentrations: 100 μ M ddA, 1 μ M GF109203X, 100 μ M IBMX, 1 μ M KT5720, 5 μ M mSIRK or mSIRK L9A, 10 μ M NF023, 10 μ M NF449, 100 nM UBO-QIC. Antagonists were pre-incubated with the cells for 10 min, and were used at 100x the K_i (100 nM ICI-118,551 and 10 nM N-methyl scopolamine). Cells were pre-treated with pertussis toxin (PTx; 100 ng/mL) at 37°C and 5% CO₂ in 0.5% FBS v/v DMEM for 16 hr.

Fluorescence imaging was performed using a high-content GE Healthcare INCell 2000 Analyzer with a Nikon Plan Fluor ELWD 40x (NA 0.6) objective and FRET module as described (89). For CFP/YFP (pmEpac2, cytoCKAR, pmCKAR, Raichu-Cdc42) emission ratio analysis, cells were sequentially excited using a CFP filter (430/24) with emission measured using YFP (535/30) and CFP (470/24) filters, and a polychroic optimized for the CFP/YFP filter pair (Quad3). For GFP/RFP (cytoEKAR, nucEKAR) emission ratio analysis, cells were sequentially excited using a FITC filter (490/20) with emission measured using dsRed (605/52) and FITC (525/36) filters, and a polychroic optimized for the FITC/dsRed filter pair (Quad4). Cells were either imaged every 20 sec for 5 min (image capture of 5 wells per 20 sec) or every 1 min for 20 min (image capture of 14 wells per min). At the end of each experiment, the same cells were stimulated with the following positive controls to maximally activate the biosensor: 10 μ M forskolin, 100 μ M IBMX with 100 nM PGE₁ for Epac2, 200 nM phorbol 12,13-dibutyrate (PDBu) for EKAR or 200 nM PDBu with phosphatase inhibitor cocktail (SigmaAldrich) for CKAR. Only HEK293 cells with >5% change in F/F_0 (FRET ratio relative to baseline for each cell) after stimulation with positive controls were selected for analysis, and the data expressed relative to the positive control (F/F_{Max}). For human cardiac fibroblasts, only cells with >3% change in F/F_0 after stimulation with positive controls were selected for analysis, and data were expressed as the F/F_0 due to the variation in responses to the positive controls. Data were analyzed using in-house scripts written for the FIJI distribution of ImageJ (94), as described (89).

Ratiometric pseudocolor images were generated as previously described (95). A multiplication factor of 10 was applied using the Ratio Plus plugin, the Green Fire Blue LUT was applied, and the Brightness and Contrast range was set to the minimum and maximum FRET ratios within the image stack. The rate of cAMP increase over 5 min (Fig. 2A) was determined by fitting the plateau of the response using an exponential equation (plateau followed by one phase association) in GraphPad Prism.

ELISA

HEK293 cells in 10 cm dishes were transfected with 3 μg pcDNA3.1, FLAG- $\beta_2\text{AR}$, FLAG- $\beta_2\text{AR}$ D3.32A, 3HA-M₃R or 3HA-M₃R D3.32A, then seeded into 48-well plates 24 hours post-transfection. 48 hours post-transfection, cells were washed with TBS (50 mM Tris pH 7.5, 150 mM NaCl), and fixed (4% paraformaldehyde in TBS, 30 min). Cells were washed in TBS, blocked (1% w/v skim milk, 0.1 M NaHCO₃; 4 h, RT with shaking), then incubated with primary antibodies overnight at 4°C (mouse anti-HA or anti-FLAG, both 1:2,000 in 0.1% w/v BSA in TBS). Cells were washed three times with TBS, then incubated with secondary goat anti-mouse-HRP antibody solution (1:2,000, 0.1% w/v BSA in TBS, 2 h, RT). SIGMAFAST™ OPD substrate solution (Sigma-Aldrich) was added and the reaction was terminated with 3M HCl. The samples were transferred to a 96-well plate and optical density at 492 nm was measured using an EnVision Multilabel Reader (PerkinElmer). Data are expressed as the fold change in receptor expression compared to pcDNA3.1 transfected cells from n biological repeats as stated.

Mathematical modeling

Model definition

The kinetics of ligand-receptor binding for a population of cells is defined by:



where i is an index denoting a particular cell, L represents free ligand, R represents the unbound receptor, B represents the occupied receptor, and k_f and k_r are association and dissociation rate constants, respectively. Activation of a cell is taken to be proportional to the number of occupied receptors:



where k_{act} is the activation rate constant, C represents an inactive cell and C^* represents an active cell. Note that C_i has a value of 1 until activation and 0 thereafter. In addition to the kinetic parameters, we introduce f_c , the fraction of cells competent to be activated by ligand. This parameter is introduced to account for any intracellular conditions (e.g. gene expression, cell cycle state etc.) that may prevent a cell from responding to ligand.

Simulation

For 1 fM Iso, we simulated the stochastic ligand-receptor binding kinetics using Gillespie's algorithm (42). This approach is not computationally feasible when considering the high ligand concentration (100 nM), because the number of reaction events per unit time scales linearly with the number of molecules in the system (120,440/well for 1 fM vs. 1.2×10^{13} /well for 100 nM). As we use molecule copy numbers in these simulations, the concentrations of biochemical species and the association rate constant, k_f , must be converted to the appropriate units:

$$\# M = [M] \cdot N_A \cdot V \quad (3)$$

$$k_{f,\#} = \frac{k_f}{N_A \cdot V} \quad (4)$$

where V is the extracellular volume (200 μ L), M is a biochemical species and N_A is the Avogadro constant. To estimate the concentration of occupied receptors ($[B]$) at high ligand concentration, we make a quasi steady-state approximation for the ligand-receptor interaction because the total ligand concentration, $[L_T]$, is much greater than the total receptor concentration, $[R_T]$:

$$[B] = [R_T] \cdot \frac{k_f [L_T]}{k_r + k_f [L_T]} \quad (5)$$

We can also calculate the average concentration of occupied receptors per cell:

$$\langle [B_i] \rangle = \frac{[B]}{N_{\text{cells}}} \quad (6)$$

The fraction of cells, F_A , that are active after a time, t , is:

$$F_A = 1 - e^{-\lambda t} \quad (7)$$

with $\lambda = k_{act} \cdot \langle [B_i] \rangle$ as the average rate of activation for each cell. For $k_{act} > 10^{-4} s^{-1}$, all cells are activated in less than 1 min when $[B] \approx [R_T]$.

Parameter estimation

We used a Bayesian approach to estimate the following parameters in our model: k_r and k_{act} , which are rate constants in the model defined above with units of s^{-1} ; K_D , which is the equilibrium dissociation constant in molar units (M) for ligand-receptor binding and can be used to calculate k_f , given k_r ; and f_c , which is the fraction of cells competent for activation (dimension-less).

Our procedure uses a Markov chain Monte Carlo (MCMC) algorithm to estimate the probability distribution of the parameters' values similar to the procedure outlined in (43). In Bayesian statistics, this estimated distribution is called a parameter's *posterior*. For each parameter set sampled during the MCMC run, estimating the posterior requires calculating both the probability of observing the experimental data given a particular set of parameters (the *likelihood*) and the probability of the parameters given an assumed probability distribution (the parameter's *prior* distribution).

Two parameters' means and standard deviations have already been characterized in the literature, $\log_{10} K_D$ (58) and k_r (96). We assign $\log_{10} K_D$ to have a normal distribution as its prior, with mean, μ , and standard deviation, σ :

$$P(\log_{10} K_D) = \text{Normal}(\mu = -9.768, \sigma = 0.612) \quad (8)$$

Assuming normality for k_r results in significant probability density for values below zero. We therefore assign k_r to have a gamma distribution as its prior, with the gamma distribution's parameters α and β calculated such that the distribution's mean, α/β , and standard deviation, $\sqrt{\alpha/\beta^2}$, correspond to the mean and standard deviation reported in the literature, 0.05 and 0.0255, respectively:

$$\frac{\alpha}{\beta} = 0.05 \quad (9)$$

$$\frac{\alpha}{\beta^2} = 0.0255^2 \quad (10)$$

$$P(k_r) = \text{Gamma}(\alpha = 3.845, \beta = 76.894) \quad (11)$$

The prior for the fraction of competent cells, f_c , can be specified based on our data as follows. We assume that 100 nM Iso is a saturating dose that should activate all competent cells, and so we calculate the mean and standard deviation of the cells that are activated in response to 100 nM Iso (Fig. 2J) and assign f_c to have the normal distribution:

$$P(f_c) = \text{Normal}(\mu = 0.711, \sigma = 0.092) \quad (12)$$

with μ and σ calculated from the data in Fig. 2J. The rate of receptor-dependent cell activation relies on incomplete knowledge of the relevant signaling pathways. However, we can still constrain this parameter with a uniformly distributed prior over a finite range. We assume that the activation rate must be sufficiently fast to activate cells given potential values of k_r , and that excessively fast activation rates are not physically realizable. Thus, we set:

$$P(\log_{10} k_{act}) = \text{Uniform}(-4, 2) \quad (13)$$

Other fixed parameters used in the model are volume of medium (200 μ L/well), number of cells (30,000/well) and number of receptors (18,000/cell; (97, 98)). Our MCMC sampling was performed for 1,000,000 iterations with a constant jump size of 0.2 (in log space), and we discarded the first 10,000 points as the burn-in period. Parameter updates were accepted using the Metropolis-Hastings criterion, with approximately 37% of the attempted updates being rejected. The sampling trace for $\log_{10} K_D$ appears to have reached stationarity (fig. S5A). From this, we can characterize the posterior distribution of each parameter; the posteriors for three of the four free parameters strongly reflect their priors (fig. S5B). The exception, k_{act} , reveals a posterior that is shifted towards larger values, with near uniformity for parameters larger than 0.01. We can further characterize the correlations between the free parameters by looking at their pairwise scatter plots (fig. S5C). All pairwise relationships result in a Spearman's rank correlation coefficient, ρ , of less than 0.05, meaning that dependency between any pair of parameters is unlikely.

Immunoblotting

Proteins were resolved by SDS-PAGE using 10% Tris-glycine or pre-cast 4-15% Mini-PROTEAN TGX gels (for AKAP250 co-IP only; Bio-Rad) and transferred to 0.45 μ m LF PVDF membranes (Bio-Rad) using a Trans-Blot SD Semi-Dry Transfer Cell (Bio-Rad; 75 min, 10 V). Membranes were blocked for 1 hour at RT (5% w/v BSA for GST pulldowns or 5% w/v skim milk powder for confirmation of protein knockdown and overexpression or co-IP, in PBS with 0.1% v/v Tween-20, PBS-T), and incubated with primary antibody overnight at 4°C (diluted in 1% w/v BSA for GST pulldowns or 1% w/v skim milk powder for confirmation of protein knockdown and overexpression or co-IP, in PBS-T). Membranes were washed, incubated with secondary antibody (diluted in PBS-T for fluorescent secondary antibodies for GST pulldowns or 1% w/v skim milk powder in PBS-T for HRP-conjugated secondary antibodies for confirmation of protein knockdown and overexpression or co-IP)

for 1 hour at RT, and washed. Immunoreactivity was detected by fluorescence for GST pulldowns (fluorescently-conjugated secondary antibodies) or ECL for confirmation of protein knockdown and overexpression or co-IP (Millipore, HRP-conjugated secondary antibodies). Fluorescence was detected using the Odyssey Classic Infrared Imager (LI-COR Biosciences), with resolution set at 169 μm and the intensity adjusted to be in the linear range for infrared fluorescence detection. ECL was detected using the ChemiDoc Touch Imaging System (Bio-Rad), with exposures adjusted to be in the linear range for chemiluminescence.

Antibodies for immunoblotting

Immunoblotting was performed using primary antibodies recognizing AKAP79 (Millipore ABS102; rabbit; 1:1,000), β -actin (Abcam ab36956; rabbit; 1:1,000), β -arrestin 1/2 (Cell Signaling 46745; rabbit; 1:1,000), β -arrestin 1 (Abcam ab31868; rabbit; 1:1,000), β -arrestin 2 (Millipore AB6022; rabbit; 1:1,000), β -tubulin (Santa Cruz Biotechnology sc-9104; rabbit; 1:5,000), $G\alpha_{i3}$ (Santa Cruz Biotechnology sc-262; rabbit; 1:1,000), $G\alpha_{q/11}$ (Santa Cruz Biotechnology sc-392; rabbit; 1:1,000), $G\alpha_s$ (Millipore 06-237; rabbit; 1:1,000), gravin (AKAP250; Sigma-Aldrich G3795; mouse; 1:1,000), GST (Sigma-Aldrich G1660; mouse; 1:25,000), HA (Abcam ab9110; rabbit; 1:5,000), PDE4D (Abcam ab14613 for GST pulldowns or Santa Cruz Biotechnology sc-25814 for confirmation of protein overexpression; rabbit; 1:1,000), PKA (Santa Cruz Biotechnology sc-903; rabbit; 1:1,000), or PKC (Millipore 05-983; mouse; 1:1,000). Immunoblotting was detected using fluorescent or HRP-conjugated secondary antibodies as follows: goat anti-mouse 680 (LI-COR 926-68070; 1:10,000), goat anti-mouse-HRP (Abcam ab97023; 1:2,000), goat anti-rabbit 800 (LI-COR 926-32211; 1:10,000), goat anti-rabbit-HRP (Cell Signaling 70745; 1:2,000 to detect β -arrestin 2, 1:5,000 to detect AKAP79, β -arrestin 1/2 and PDE4D).

Confirmation of protein knockdown and dominant negative overexpression

HEK293 cells were seeded into 6-well plates and grown to 70% confluency. Cells were transfected with 25 nM scrambled or targeted siRNA or 1.5 µg pcDNA/pSilencer, targeted shRNA or dominant negative cDNA for 72 hours using PEI. Following transfection, cells were lysed in 100 µL modified RIPA lysis buffer (50 mM Tris pH 7.4, 375 mM NaCl, 1 mM EDTA, 1% v/v Triton X-100, 0.5% w/v sodium deoxycholate, 0.1% w/v SDS) for 30 min on ice. Lysates were centrifuged (10,000g, 15 min, 4°C), and protein concentration in the supernatant determined using the Bradford Ultra reagent (Expedeon). Laemmli sample buffer was added to the supernatants, and samples incubated at 37°C for 30 min prior to immunoblotting.

GST pulldowns

GST-tagged fragments were expressed in BL21(DE3)pLys cells at 37°C following induction with 0.1 mM IPTG. Cells were lysed by sonication (three pulses for 30 sec, 70% amplitude; Qsonica Q125) in lysis buffer (50 mM Tris pH 8, 300 mM NaCl, 10 mM MgCl₂, 1 mM EDTA, 1 mM DTT, 0.25 mg/mL lysozyme, protease inhibitor cocktail, 100 U DNaseI). The homogenates were centrifuged (15,000g, 20 min, 4°C) and the supernatants incubated with Glutathione Sepharose 4B resin (GE Healthcare; 1 h, 4°C). The resin was washed (50 mM Tris pH 8, 150 mM NaCl, 1 mM EDTA, 1 mM DTT) until no protein remained in the eluate, then an equal volume of PBS (with protease inhibitors and 0.02% w/v NaN₃) was added to the resin.

HEK293 cells were seeded into 175 cm² flasks and grown to confluency. For over-expression pull-downs, cells were transfected with 20 µg AKAP79-HA, PDE4D3 dn, PDE4D5 dn, AC2-HA or HA-AKAP250 using PEI. Cells were lysed in lysis buffer (50 mM Tris pH 7.4, 100 mM NaCl, 10% v/v glycerol, 0.3% v/v NP-40, 2 mM DTT, 1 mM PMSF, 1 mM benzamide, 10 mM β-

glycerophosphate, 2 mM Na₃VO₄, protease inhibitor cocktail, 100 U DNaseI) by rotating for 30 min at 4°C, then passing 10 times through a 21-gauge needle. The cell homogenates were centrifuged (500g, 3 min, 4°C), then incubated with the GST-β₂AR or GST-M₃R fragment resin for 4 hours at 4°C with rotation. The GST-β₂AR or GST-M₃R fragment resin was washed twice in lysis buffer (with 0.03% v/v NP-40), before the bound proteins were eluted in Laemmli buffer and incubated at 37°C for 30 min prior to immunoblotting. Immunoreactive bands were quantified by densitometry using Image Studio Lite 4.0 software (LI-COR Biosciences). Data for each fragment are normalized for equivalent amounts of GST, and expressed relative to GST alone control from *n* biological repeats as stated.

Co-immunoprecipitation (co-IP)

HEK293 cells in 175 cm² flasks were transfected with 20 μg HA-AKAP250 using PEI. 48 hr post-transfection, cells from eight flasks were lysed in modified lysis buffer (50 mM Tris pH 7.4, 100 mM NaCl, 10% v/v glycerol, 1% v/v Triton X-100, 0.5% v/v NP-40, 2 mM DTT, 1 mM PMSF, 1 mM benzamidine, 10 mM β-glycerophosphate, 2 mM Na₃VO₄, protease inhibitor cocktail, 100 U DNaseI) by rotating at 4°C for 20 min. The cell homogenates were centrifuged (16,000g, 10 min, 4°C), then halved and incubated with anti-HA affinity matrix (Roche Life Science) overnight at 4°C with rotation. The anti-HA affinity matrix was washed three times in lysis buffer, before the bound proteins were eluted in Laemmli buffer and incubated at 37°C for 30 min prior to immunoblotting.

Acceptor photobleaching FRET

HEK293 cells were seeded in 6-well plates and grown to 70% confluency prior to co-transfection with 0.6 μg/well FLAG-β₂AR-CFP or 3HA-M₃R-CFP and 0.6 μg/well of one of the following YFP-tagged proteins: Gα_s-YFP, Gα_q-YFP, AKAP79-YFP, YFP-β-arrestin 1, YFP-β-arrestin 2, YFP-PKC or PKA-YFP. The FRET biosensor, pmEpac2, was used as a positive control. 4 hours post-transfection, cells

were re-seeded (40,000 cells/well) into a 8-well μ -slide (iBidi). 24 hours post-transfection, cells were rinsed in PBS, fixed (4% w/v paraformaldehyde, 30 min at RT), rinsed three times in PBS, then stored at 4°C.

Acceptor photobleaching FRET was performed using a Leica SP8 confocal microscope with HCX PL APO 63x CS2 (NA 1.40) oil objective using the FRET Acceptor Photobleaching wizard in the LAS X software suite. A region of interest (ROI) was selected, and the acceptor channel bleached at 70% laser intensity (514 nm) until the YFP signal was reduced by at least 90%. CFP (UV 405 nm laser excitation, 465-511 nm emission) and YFP (514 nm laser excitation, 532-603 nm emission) emission was then measured. For each biological replicate, three cells and two ROIs per cell were analysed (total 24 ROIs from four biological replicates). FRET efficiency was calculated by the LAS X software suite using the following equation: $\text{FRET}_{\text{eff}} = (\text{Donor}_{\text{post}} - \text{Donor}_{\text{pre}}) / \text{Donor}_{\text{post}}$. $\text{G}\alpha_{\text{q}}$ -YFP and $\text{G}\alpha_{\text{s}}$ -YFP were used as negative controls for FLAG- β_2 AR-CFP and 3HA-M₃R-CFP FRET, respectively. Due to non-uniform distribution of protein complexes at the plasma membrane, and a large number of “0” FRET values, the data was not normally distributed and was therefore statistically analysed using a non-parametric Kruskal-Wallis test. For further analysis, data were converted to binary values (0 = no FRET, 1 = FRET) and analysed using a Chi-square test with two-sided P-values and 95% confidence interval.

LC-MS/MS: FASP protein digestion and dimethyl labeling

HEK293 cells were seeded in 6-well plates and grown to confluency. Cells were treated with vehicle or ligand for 4 h, then incubated in lysis buffer (100 mM Tris pH 7.6, 4% w/v SDS, 100 mM DTT) at 95°C for 3 min, prior to sonication (30 sec, 30% amplitude, Qsonica Q125) and centrifugation (16,000g, 5 min, RT). 100 μ g supernatant was digested using the FASP Protein Digestion Kit (Expedeon), with trypsin digestion overnight at 37°C. Digested peptides were labeled as previously

described (99) using 40 mM $^{12}\text{C}_3$ light or $^{13}\text{C}_3$ heavy formaldehyde with 20 mM NaCNBOH for 1 hour at 37°C, before the reaction was quenched with formic acid (to pH 2.5). The light- and heavy-labeled samples were mixed at a 1:1 ratio, and desalted using C-18 desalting columns and three washes with 0.1% v/v formic acid. Samples were eluted in 70% v/v acetonitrile and 0.1% v/v formic acid, then dried by SpeedVac (LABCONCO). Peptides were fractionated following resuspension in Strong Anion Exchange (SAX) buffer (20 mM acetic acid, 20 mM phosphoric acid, 20 mM boric acid) pH 11 and loading onto stage tips containing five layers of anion exchange discs. The first fraction was collected following centrifugation (1,000g, 3 min, RT). A total of seven fractions were collected by sequentially eluting fractions from the stage tips in SAX buffer at pH 8, 6, 5, 4, 3 and SAX buffer 7 (10% v/v formic acid, pH 1). Fractions were dried, then resuspended in 2% v/v acetonitrile with 1% v/v formic acid by sonication at 37°C for 10 min prior to LC-MS/MS.

Proteomic analysis by LC-MS/MS: Data collection and analysis

Samples were analyzed by LC-MS/MS using a Q ExactiveTM or Q Exactive PlusTM Orbitrap mass spectrometer (Thermo Scientific) coupled online with an UltiMate 3000 RSLC nano-UHPLC (Thermo Scientific). Samples were injected onto an AcclaimTM PepMap100 RSLC C18 analytical column (100 Å pore size, 75 µm i.d. x 50 cm reversed phase nanoViper column, Thermo Scientific) with 95% buffer A (0.1% v/v formic acid) at a flow rate of 250 or 300 nL/min. The peptides were eluted over 60 min using a gradient to 42.5% buffer B (80% v/v acetonitrile, 0.1% v/v formic acid). The eluate was nebulized and ionized using a Nano ElectroSpray Ion Source (Thermo Scientific) with coated borosilicate emitter and a capillary voltage of 1700 V. Peptides were selected for MS/MS analysis using XcaliburTM software (Thermo Scientific) in full MS/dd-MS² (TopN) mode with the following parameter settings: MS AGC target 3E6, MS maximum injection time 120 ms, MS/MS TopN=10 or 12, MS/MS AGC target 1e5, MS/MS maximum injection time 120 ms, normalized collision energy 27,

and isolation window of 2 or 1.8 m/z. Dynamic exclusion was set to 15 sec. Protein identification and quantification was performed using MaxQuant software (100) (version 1.5.3.17). Searches were performed against human sequences downloaded from UniProt (101) (August 2015 version) using the following parameters: specific digestion with trypsin with up to two missed cleavages, protein N-terminal acetylation and methionine oxidation were set as variable modifications, and cysteine alkylation was set as a fixed modification.

Data were analyzed using Perseus software (version 1.5.0.15). Common contaminants, reverse peptides, and proteins identified only by a modification site were removed. All data were expressed relative to vehicle-treated controls (heavy/light or transformed 1/[heavy/light], as appropriate), ratios were \log_2 normalized to allow quantitative analysis, and any non-valid values removed. Only proteins that differed significantly from vehicle controls (t-test with $p < 0.05$) were retained and Z-scored to prepare the data for clustering. Hierarchical clustering was performed using default settings. Data for individual proteins are expressed as the \log_2 change relative to vehicle control from n biological repeats as stated.

The proteins used for hierarchical clustering were further classified by their Biological Process GeneOntology (GO) term, using the Database for Annotation, Visualization and Integrated Discovery (DAVID, v6.7) (102, 103) to generate pie charts. Classifications with p-values < 0.05 were used to group proteins according to biological function, synonymous classifications were removed, and the number of proteins classified within these groups were counted. Only classifications that were identified in at least two biological replicates were included within the final count.

High-content EF1 α -GFP imaging

HEK293 cells were seeded in black, optically clear 96-well plates and grown to 70% confluency prior to co-transfection with 50 ng/well pEF1 α -AcGFP-C1 and 50 ng/well pDsRed-N1 (transfection efficiency control) using PEI. 24 hours post transfection, cells were washed with PBS and partially serum restricted in phenol red-free DMEM supplemented with 0.5% FBS v/v overnight. Human cardiac fibroblasts were transfected with 50 ng/well pEF1 α -AcGFP-C1 and 50 ng/well pDsRed-N1 (transfection efficiency control) using X-tremeGENE 9 in suspension, then seeded in black, optically clear 96-well plates at 90% confluency. Experiments in human cardiac fibroblasts used HBSS.

Fluorescence imaging was performed using a high-content GE Healthcare INCell 2000 Analyzer with a Nikon Plan Fluor ELWD 40x (NA 0.6) objective. Sequential GFP/dsRed imaging used FITC (excitation 490/20, emission 525/36) and dsRed (excitation 555/25, emission 605/52) filters and the Quad4 polychroic. Baseline images were taken every 10 min for 40 min, cells were stimulated with ligand and images taken every 10 min for 4 hr. Data were analyzed by selecting 70 cells per well using FIJI, and the GFP fluorescence intensity was expressed relative to the average baseline GFP fluorescence intensity for each cell (F/F_0). For human cardiac fibroblasts, all transfected cells were selected and data are expressed as relative fluorescence units (RFU) due to variation in transfection efficiency.

Statistics

All data points are the mean \pm S.E.M. of at least three independent experiments unless otherwise stated. All data were analyzed using GraphPad Prism with statistically significant differences ($p < 0.05$) determined using Kruskal-Wallis or Chi-square analysis (acceptor photobleaching FRET) or one- or two-way ANOVAs (all other experiments) with appropriate post-tests, as stated.

Supplementary Materials

Figure S1. Endogenous expression of transcripts encoding GPCRs in HEK293 cells.

Figure S2. Biphasic changes in cAMP are due to activation of endogenous β_2 AR and M_3 R.

Figure S3. FRET biosensors can detect responses of endogenous or exogenous receptors to femtomolar concentrations of ligand.

Figure S4. Plasma membrane localization and activity of mutant β_2 AR and M_3 R.

Figure S5. Modeling responses to femtomolar concentrations of isopreterenol.

Figure S6. Identification of proteins involved in mediating responses to 1 fM isopreterenol.

Figure S7. The β_2 AR forms a pre-assembled signalling complex.

Figure S8. Identification of proteins involved in mediating responses to 1 fM carbachol.

Figure S9. The M_3 R forms a pre-assembled signalling complex.

Figure S10. Femtomolar ligand concentrations activate compartmentalised signalling and unique cell responses.

Table S1. Femtomolar concentrations of ligand increase cAMP.

Table S2. The β_2 AR and M_3 R constitutively form complexes at the plasma membrane.

Table S3. Proteins from hierarchical clustering analysis.

References and Notes

1. M. Audet, M. Bouvier, Insights into signaling from the β 2-adrenergic receptor structure, *Nat Chem Biol* **4**, 397–403 (2008).
2. N. G. Tsvetanova, M. von Zastrow, Spatial encoding of cyclic AMP signaling specificity by GPCR endocytosis, *Nat Chem Biol* **10**, 1061–1065 (2014).
3. I. D. C. Fraser, M. Cong, J. Kim, E. N. Rollins, Y. Daaka, R. J. Lefkowitz, J. D. Scott, Assembly of an A kinase-anchoring protein– β 2-adrenergic receptor complex facilitates receptor phosphorylation and signaling, *Curr Biol* **10**, 409–412 (2000).
4. D. Calebiro, V. O. Nikolaev, M. C. Gagliani, T. de Filippis, C. Dees, C. Tacchetti, L. Persani, M. J. Lohse, Persistent cAMP-signals triggered by internalized G-protein-coupled receptors, *PLoS Biol* **7**, e1000172 (2009).
5. M. J. Lynch, G. S. Baillie, A. Mohamed, X. Li, C. Maisonneuve, E. Klusmann, G. van Heeke, M. D. Houslay, RNA silencing identifies PDE4D5 as the functionally relevant cAMP phosphodiesterase interacting with β arrestin to control the protein kinase A/AKAP79-mediated switching of the β 2-adrenergic receptor to activation of ERK in HEK293B2 cells, *J Biol Chem* **280**, 33178–33189 (2005).
6. M. Shih, F. Lin, J. D. Scott, H.-Y. Wang, C. C. Malbon, Dynamic complexes of β 2-adrenergic receptors with protein kinases and phosphatases and the role of gravin, *J Biol Chem* **274**, 1588–1595 (1999).
7. J. X. Shen, D. M. F. Cooper, AKAP79, PKC, PKA and PDE4 participate in a Gq-linked muscarinic receptor and adenylate cyclase 2 cAMP signalling complex, *Biochem J* **455**, 47–56 (2013).
8. M. L. Halls, D. M. F. Cooper, Sub-picomolar relaxin signalling by a pre-assembled RXFP1, AKAP79, AC2, β -arrestin 2, PDE4D3 complex, *EMBO J* **29**, 2772–2787 (2010).
9. D. D. Jensen, T. Lieu, M. L. Halls, N. A. Veldhuis, W. L. Imlach, Q. N. Mai, D. P. Poole, T. Quach, L. Aurelio, J. Conner, C. K. Herenbrink, N. Barlow, J. S. Simpson, M. J. Scanlon, B. Graham, A. McCluskey, P. J. Robinson, V. Escriou, R. Nassini, S. Materazzi, P. Geppetti, G. A. Hicks, M. J. Christie, C. J. H. Porter, M. Canals, N. W. Bunnett, Neurokinin 1 receptor signaling in endosomes mediates sustained nociception and is a viable therapeutic target for prolonged pain relief, *Sci Transl Med* **9**, pii: eaal3447 (2017).
10. R. E. Yarwood, W. L. Imlach, T. Lieu, N. A. Veldhuis, D. D. Jensen, C. Klein Herenbrink, L. Aurelio, Z. Cai, M. J. Christie, D. P. Poole, C. J. H. Porter, P. McLean, G. A. Hicks, P. Geppetti, M. L. Halls, M. Canals, N. W. Bunnett, Endosomal signaling of the receptor for calcitonin gene-related peptide mediates pain transmission, *Proc Natl Acad Sci USA* **114**, 12309–12314 (2017).
11. V. O. Nikolaev, M. Bünemann, E. Schmitteckert, M. J. Lohse, S. Engelhardt, Cyclic AMP imaging in adult cardiac myocytes reveals far-reaching β 1-adrenergic but locally confined β 2-adrenergic receptor-mediated signaling, *Circ Res* **99**, 1084–1091 (2006).
12. R. Irannejad, J. C. Tomshine, J. R. Tomshine, M. Chevalier, J. P. Mahoney, J. Steyaert, S. G. F. Rasmussen, R. K. Sunahara, H. El-Samad, B. Huang, M. von Zastrow, Conformational biosensors reveal GPCR signalling from endosomes, *Nature* **495**, 534–538 (2013).

13. K. A. DeFea, β -arrestins as regulators of signal termination and transduction: how do they determine what to scaffold? *Cell Signal* **23**, 621–629 (2011).
14. S. Ferrandon, T. N. Feinstein, M. Castro, B. Wang, R. Bouley, J. T. Potts, T. J. Gardella, J.-P. Vilardaga, Sustained cyclic AMP production by parathyroid hormone receptor endocytosis, *Nat Chem Biol* **5**, 734–742 (2009).
15. V. L. Wehbi, H. P. Stevenson, T. N. Feinstein, G. Calero, G. Romero, J.-P. Vilardaga, Noncanonical GPCR signaling arising from a PTH receptor-arrestin-G $\beta\gamma$ complex, *Proc Natl Acad Sci USA* **110**, 1530–1535 (2013).
16. T. N. Feinstein, V. L. Wehbi, J. A. Ardura, D. S. Wheeler, S. Ferrandon, T. J. Gardella, J.-P. Vilardaga, Retromer terminates the generation of cAMP by internalized PTH receptors, *Nat Chem Biol* **7**, 278–284 (2011).
17. S. J. Kotowski, F. W. Hopf, T. Seif, A. Bonci, M. von Zastrow, Endocytosis promotes rapid dopaminergic signaling, *Neuron* **71**, 278–290 (2011).
18. C. A. Dinarello, The interleukin-1 family: 10 years of discovery, *FASEB J* **8**, 1314–1325 (1994).
19. A. Bruzzone, A. Saulière, F. Finana, J.-M. Sénard, I. Lüthy, C. Gales, Dosage-dependent regulation of cell proliferation and adhesion through dual β 2-adrenergic receptor/cAMP signals, *FASEB J* **28**, 1342–1354 (2014).
20. R. A. Ngala, J. O'Dowd, S. J. Wang, C. Stocker, M. A. Cawthorne, J. R. S. Arch, β 2-adrenoceptors and non-beta-adrenoceptors mediate effects of BRL37344 and clenbuterol on glucose uptake in soleus muscle: studies using knockout mice, *Br J Pharmacol* **158**, 1676–1682 (2009).
21. R. A. Ngala, J. O'Dowd, S. J. Wang, A. Agarwal, C. Stocker, M. A. Cawthorne, J. R. S. Arch, Metabolic responses to BRL37344 and clenbuterol in soleus muscle and C2C12 cells via different atypical pharmacologies and β 2-adrenoceptor mechanisms, *Br J Pharmacol* **155**, 395–406 (2008).
22. L. Block, J. Forshammar, A. Westerlund, U. Björklund, C. Lundborg, B. Biber, E. Hansson, Naloxone in ultralow concentration restores endomorphin-1-evoked Ca²⁺ signaling in lipopolysaccharide pretreated astrocytes, *Neuroscience* **205**, 1–9 (2012).
23. B. Liu, L. Qin, S. N. Yang, B. C. Wilson, Y. Liu, J. S. Hong, Femtomolar concentrations of dynorphins protect rat mesencephalic dopaminergic neurons against inflammatory damage, *J Pharmacol Exp Ther* **298**, 1133–1141 (2001).
24. S. M. Crain, K. F. Shen, Ultra-low concentrations of naloxone selectively antagonize excitatory effects of morphine on sensory neurons, thereby increasing its antinociceptive potency and attenuating tolerance/dependence during chronic cotreatment, *Proc Natl Acad Sci USA* **92**, 10540–10544 (1995).
25. M. R. Goldberg, P. D. Joiner, A. L. Hyman, P. J. Kadowitz, Unusual vasoconstrictor effects of angiotensin II, *Proc Soc Exp Biol Med* **149**, 707–713 (1975).
26. S. C. Kuttan, M. K. Sim, Endothelium-dependent response of the rabbit aorta to femtomolar concentrations of angiotensin II, *J Cardiovasc Pharmacol* **17**, 929–934 (1991).

27. Y. Sun, J. Huang, Y. Xiang, M. Bastepe, H. Jüppner, B. K. Kobilka, J. J. Zhang, X.-Y. Huang, Dosage-dependent switch from G protein-coupled to G protein-independent signaling by a GPCR, *EMBO J* **26**, 53–64 (2007).
28. M. Uhlén, L. Fagerberg, B. M. Hallström, C. Lindskog, P. Oksvold, A. Mardinoglu, Å. Sivertsson, C. Kampf, E. Sjöstedt, A. Asplund, I. Olsson, K. Edlund, E. Lundberg, S. Navani, C. A.-K. Szigartyo, J. Odeberg, D. Djureinovic, J. O. Takanen, S. Hober, T. Alm, P.-H. Edqvist, H. Berling, H. Tegel, J. Mulder, J. Rockberg, P. Nilsson, J. M. Schwenk, M. Hamsten, K. von Feilitzen, M. Forsberg, L. Persson, F. Johansson, M. Zwahlen, G. von Heijne, J. Nielsen, F. Pontén, Proteomics. Tissue-based map of the human proteome, *Science* **347**, 1260419 (2015).
29. B. K. Atwood, J. Lopez, J. Wager-Miller, K. Mackie, A. Straiker, Expression of G protein-coupled receptors and related proteins in HEK293, AtT20, BV2, and N18 cell lines as revealed by microarray analysis, *BMC Genomics* **12**, 14 (2011).
30. X. M. van Wijk, S. Döhrmann, B. M. Hallström, S. Li, B. G. Voldborg, B. X. Meng, K. K. McKee, T. H. van Kuppevelt, P. D. Yurchenco, B. O. Palsson, N. E. Lewis, V. Nizet, J. D. Esko, Whole-genome sequencing of invasion-resistant cells identifies laminin $\alpha 2$ as a host factor for bacterial invasion, *MBio* **8**, pii: e02128-16 (2017).
31. J. Yang, W. S. Hlavacek, Scaffold-mediated nucleation of protein signaling complexes: elementary principles, *Math Biosci* **232**, 164–173 (2011).
32. S. Wachten, N. Masada, L.-J. Ayling, A. Ciruela, V. O. Nikolaev, M. J. Lohse, D. M. F. Cooper, Distinct pools of cAMP centre on different isoforms of adenylyl cyclase in pituitary-derived GH3B6 cells, *J Cell Sci* **123**, 95–106 (2010).
33. T. Nakakuki, M. R. Birtwistle, Y. Saeki, N. Yumoto, K. Ide, T. Nagashima, L. Bruschi, B. A. Ogunnaike, M. Okada-Hatakeyama, B. N. Kholodenko, Ligand-specific c-Fos expression emerges from the spatiotemporal control of ErbB network dynamics, *Cell* **141**, 884–896 (2010).
34. M. Canals, P. M. Sexton, A. Christopoulos, Allostery in GPCRs: “MWC” revisited, *Trends Biochem Sci* **36**, 663–672 (2011).
35. R. O. Dror, A. C. Pan, D. H. Arlow, D. W. Borhani, P. Maragakis, Y. Shan, H. Xu, D. E. Shaw, Pathway and mechanism of drug binding to G-protein-coupled receptors, *Proc Natl Acad Sci USA* **108**, 13118–13123 (2011).
36. A. C. Kruse, J. Hu, A. C. Pan, D. H. Arlow, D. M. Rosenbaum, E. Rosemond, H. F. Green, T. Liu, P. S. Chae, R. O. Dror, D. E. Shaw, W. I. Weis, J. Wess, B. K. Kobilka, Structure and dynamics of the M3 muscarinic acetylcholine receptor, *Nature* **482**, 552–556 (2012).
37. J. A. Ballesteros, H. Weinstein, S. C. Sealfon, Ed. Integrated methods for the construction of three-dimensional models and computational probing of structure-function relations in G protein-coupled receptors, *Methods Neurosci* **25**, 366–428 (1995).
38. C. D. Strader, I. S. Sigal, M. R. Candelore, E. Rands, W. S. Hill, R. A. Dixon, Conserved aspartic acid residues 79 and 113 of the β -adrenergic receptor have different roles in receptor function, *J Biol Chem* **263**, 10267–10271 (1988).

39. C. M. Fraser, C. D. Wang, D. A. Robinson, J. D. Gocayne, J. C. Venter, Site-directed mutagenesis of m1 muscarinic acetylcholine receptors: conserved aspartic acids play important roles in receptor function, *Mol Pharmacol* **36**, 840–847 (1989).
40. B. N. Armbruster, X. Li, M. H. Pausch, S. Herlitze, B. L. Roth, Evolving the lock to fit the key to create a family of G protein-coupled receptors potently activated by an inert ligand, *Proc Natl Acad Sci USA* **104**, 5163–5168 (2007).
41. E. Alvarez-Curto, R. Prihandoko, C. S. Tautermann, J. M. Zwier, J. D. Pediani, M. J. Lohse, C. Hoffmann, A. B. Tobin, G. Milligan, Developing chemical genetic approaches to explore G protein-coupled receptor function: validation of the use of a receptor activated solely by synthetic ligand (RASSL), *Mol Pharmacol* **80**, 1033–1046 (2011).
42. D. T. Gillespie, Stochastic simulation of chemical kinetics, *Annu Rev Phys Chem* **58**, 35–55 (2007).
43. N. Kozar, D. Barua, S. Orchard, E. C. Nice, A. W. Burgess, W. S. Hlavacek, A. H. A. Clayton, Exploring higher-order EGFR oligomerisation and phosphorylation--a combined experimental and theoretical approach, *Mol Biosyst* **9**, 1849–1863 (2013).
44. A. Strasser, H.-J. Wittmann, R. Seifert, Binding kinetics and pathways of ligands to GPCRs, *Trends Pharmacol Sci* **38**, 717–732 (2017).
45. M. J. Lynch, G. S. Baillie, M. D. Houslay, cAMP-specific phosphodiesterase-4D5 (PDE4D5) provides a paradigm for understanding the unique non-redundant roles that PDE4 isoforms play in shaping compartmentalized cAMP cell signalling, *Biochem Soc Trans* **35**, 938–941 (2007).
46. S. J. MacKenzie, G. S. Baillie, I. McPhee, C. MacKenzie, R. Seamons, T. McSorley, J. Millen, M. B. Beard, G. van Heeke, M. D. Houslay, Long PDE4 cAMP specific phosphodiesterases are activated by protein kinase A-mediated phosphorylation of a single serine residue in Upstream Conserved Region 1 (UCR1), *Br J Pharmacol* **136**, 421–433 (2002).
47. M. L. Halls, D. M. F. Cooper, Regulation by Ca²⁺-signaling pathways of adenylyl cyclases, *Cold Spring Harb Perspect Biol* **3**, a004143 (2011).
48. S. Gao, H.-Y. Wang, C. C. Malbon, AKAP5 and AKAP12 form homo-oligomers, *J Mol Signal* **6**, 3 (2011).
49. C. D. Harvey, A. G. Ehrhardt, C. Cellurale, H. Zhong, R. Yasuda, R. J. Davis, K. Svoboda, A genetically encoded fluorescent sensor of ERK activity, *Proc Natl Acad Sci USA* **105**, 19264–19269 (2008).
50. J. D. Violin, J. Zhang, R. Y. Tsien, A. C. Newton, A genetically encoded fluorescent reporter reveals oscillatory phosphorylation by protein kinase C, *J Cell Biol* **161**, 899–909 (2003).
51. L. L. Gallegos, M. T. Kunkel, A. C. Newton, Targeting protein kinase C activity reporter to discrete intracellular regions reveals spatiotemporal differences in agonist-dependent signaling, *J Biol Chem* **281**, 30947–30956 (2006).

52. R. E. Itoh, K. Kurokawa, Y. Ohba, H. Yoshizaki, N. Mochizuki, M. Matsuda, Activation of rac and cdc42 video imaged by fluorescent resonance energy transfer-based single-molecule probes in the membrane of living cells, *Mol Cell Biol* **22**, 6582–6591 (2002).
53. Y. Takai, T. Sasaki, T. Matozaki, Small GTP-binding proteins, *Physiol Reviews* **81**, 153–208 (2001).
54. G. Vauquelin, S. J. Charlton, Long-lasting target binding and rebinding as mechanisms to prolong in vivo drug action, *Br J Pharmacol* **161**, 488–508 (2010).
55. D. A. Sykes, C. Parry, J. Reilly, P. Wright, R. A. Fairhurst, S. J. Charlton, Observed drug-receptor association rates are governed by membrane affinity: the importance of establishing “micro-pharmacokinetic/pharmacodynamic relationships” at the β 2-adrenoceptor, *Mol Pharmacol* **85**, 608–617 (2014).
56. K. Gherbi, S. J. Briddon, S. J. Charlton, Micro-pharmacokinetics: Quantifying local drug concentration at live cell membranes, *Sci Rep* **8**, 3479 (2018).
57. S. Gao, H.-Y. Wang, C. C. Malbon, AKAP12 and AKAP5 form higher-order hetero-oligomers, *J Mol Signal* **6**, 8 (2011).
58. D. P. Staus, R. T. Strachan, A. Manglik, B. Pani, A. W. Kahsai, T. H. Kim, L. M. Wingler, S. Ahn, A. Chatterjee, A. Masoudi, A. C. Kruse, E. Pardon, J. Steyaert, W. I. Weis, R. S. Prosser, B. K. Kobilka, T. Costa, R. J. Lefkowitz, Allosteric nanobodies reveal the dynamic range and diverse mechanisms of G-protein-coupled receptor activation, *Nature* **535**, 448–452 (2016).
59. N. Hoshi, L. K. Langeberg, C. M. Gould, A. C. Newton, J. D. Scott, Interaction with AKAP79 modifies the cellular pharmacology of PKC, *Mol Cell* **37**, 541–550 (2010).
60. N. Hoshi, L. K. Langeberg, J. D. Scott, Distinct enzyme combinations in AKAP signalling complexes permit functional diversity, *Nat Cell Biol* **7**, 1066–1073 (2005).
61. J. X. Shen, S. Wachten, M. L. Halls, K. L. Everett, D. M. F. Cooper, Muscarinic receptors stimulate AC2 by novel phosphorylation sites, whereas G β γ subunits exert opposing effects depending on the G-protein source, *Biochem J* **447**, 393–405 (2012).
61. G. Fan, E. Shumay, H. Wang, C. C. Malbon, The scaffold protein gravin (cAMP-dependent protein kinase-anchoring protein 250) binds the β 2-adrenergic receptor via the receptor cytoplasmic Arg-329 to Leu-413 domain and provides a mobile scaffold during desensitization, *J Biol Chem* **276**, 24005–24014 (2001).
62. M. Cong, S. J. Perry, F. T. Lin, I. D. Fraser, L. A. Hu, W. Chen, J. A. Pitcher, J. D. Scott, R. J. Lefkowitz, Regulation of membrane targeting of the G protein-coupled receptor kinase 2 by protein kinase A and its anchoring protein AKAP79, *J Biol Chem* **276**, 15192–15199 (2001).
63. I. Torrecilla, E. J. Spragg, B. Poulin, P. J. McWilliams, S. C. Mistry, A. Blaukat, A. B. Tobin, Phosphorylation and regulation of a G protein-coupled receptor by protein kinase CK2, *J Cell Biol* **177**, 127–137 (2007).

64. G. Wu, G. S. Bogatkevich, Y. V. Mukhin, J. L. Benovic, J. D. Hildebrandt, S. M. Lanier, Identification of G $\beta\gamma$ binding sites in the third intracellular loop of the M₃-muscarinic receptor and their role in receptor regulation, *J Biol Chem* **275**, 9026–9034 (2000).
65. D. O. Borroto-Escuela, P. A. Correia, W. Romero-Fernandez, M. Narvaez, K. Fuxe, F. Ciruela, P. Garriga, Muscarinic receptor family interacting proteins: role in receptor function, *J Neurosci Methods* **195**, 161–169 (2011).
66. W. Kan, M. Adjobo-Hermans, M. Burroughs, G. Faibis, S. Malik, G. G. Tall, A. V. Smrcka, M₃ muscarinic receptor interaction with phospholipase C β 3 determines its signaling efficiency, *J Biol Chem* **289**, 11206–11218 (2014).
67. J. Hu, D. Thor, Y. Zhou, T. Liu, Y. Wang, S. M. McMillin, R. Mistry, R. A. J. Challiss, S. Costanzi, J. Wess, Structural aspects of M₃ muscarinic acetylcholine receptor dimer formation and activation, *FASEB J* **26**, 604–616 (2012).
68. S. G. F. Rasmussen, B. T. DeVree, Y. Zou, A. C. Kruse, K. Y. Chung, T. S. Kobilka, F. S. Thian, P. S. Chae, E. Pardon, D. Calinski, J. M. Mathiesen, S. T. A. Shah, J. A. Lyons, M. Caffrey, S. H. Gellman, J. Steyaert, G. Skiniotis, W. I. Weis, R. K. Sunahara, B. K. Kobilka, Crystal structure of the β 2 adrenergic receptor-Gs protein complex, *Nature* **477**, 549–555 (2011).
69. A. K. Shukla, G. H. Westfield, K. Xiao, R. I. Reis, L.-Y. Huang, P. Tripathi-Shukla, J. Qian, S. Li, A. Blanc, A. N. Oleskie, A. M. Dosey, M. Su, C.-R. Liang, L.-L. Gu, J.-M. Shan, X. Chen, R. Hanna, M. Choi, X. J. Yao, B. U. Klink, A. W. Kahsai, S. S. Sidhu, S. Koide, P. A. Penczek, A. A. Kossiakoff, V. L. Woods, B. K. Kobilka, G. Skiniotis, R. J. Lefkowitz, Visualization of arrestin recruitment by a G-protein-coupled receptor, *Nature* **512**, 218–222 (2014).
70. A. R. B. Thomsen, B. Plouffe, T. J. Cahill, A. K. Shukla, J. T. Tarrasch, A. M. Dosey, A. W. Kahsai, R. T. Strachan, B. Pani, J. P. Mahoney, L. Huang, B. Breton, F. M. Heydenreich, R. K. Sunahara, G. Skiniotis, M. Bouvier, R. J. Lefkowitz, GPCR-G protein- β -arrestin super-complex mediates sustained G protein signaling, *Cell* **166**, 907–919 (2016).
71. C. E. Outten, T. V. O'Halloran, Femtomolar sensitivity of metalloregulatory proteins controlling zinc homeostasis, *Science* **292**, 2488–2492 (2001).
72. J. Draper, K. Karplus, K. M. Ottemann, Identification of a chemoreceptor zinc-binding domain common to cytoplasmic bacterial chemoreceptors, *J Bacteriol* **193**, 4338–4345 (2011).
73. F. Zähringer, E. Lacanna, U. Jenal, T. Schirmer, A. Boehm, Structure and signaling mechanism of a zinc-sensory diguanylate cyclase, *Structure* **21**, 1149–1157 (2013).
74. S. P. Skaar, The battle for iron between bacterial pathogens and their vertebrate hosts, *PLoS Pathog* **6**, e1000949 (2010).
75. K. N. Raymond, E. A. Dertz, S. S. Kim, Enterobactin: an archetype for microbial iron transport, *Proc Natl Acad Sci USA* **100**, 3584–3588 (2003).
76. W. R. Harris, C. J. Carrano, S. R. Cooper, S. R. Sofen, A. E. Avdeef, J. V. McArdle, K. N. Raymond, Coordination chemistry of microbial iron transport compounds. 19. Stability constants and

- electrochemical behavior of ferric enterobactin and model complexes, *J Am Chem Soc* **101**, 6097-6104 (1979).
77. L. D. Loomis, K. N. Raymond, Solution equilibria of enterobactin and metal-enterobactin complexes, *Inorg Chem* **30**, 906-911 (1991).
78. D. Willoughby, N. Masada, S. Wachten, M. Pagano, M. L. Halls, K. L. Everett, A. Ciruela, D. M. F. Cooper, AKAP79/150 interacts with AC8 and regulates Ca²⁺-dependent cAMP synthesis in pancreatic and neuronal systems, *J Biol Chem* **285**, 20328–20342 (2010).
79. N. Dehvari, D. S. Hutchinson, J. Nevzorova, O. S. Dallner, M. Sato, M. Kocan, J. Merlin, B. A. Evans, R. J. Summers, T. Bengtsson, $\beta(2)$ -Adrenoceptors increase translocation of GLUT4 via GPCR kinase sites in the receptor C-terminal tail, *Br J Pharmacol* **165**, 1442–1456 (2012).
80. Y. Tang, L. A. Hu, W. E. Miller, N. Ringstad, R. A. Hall, J. A. Pitcher, P. DeCamilli, R. J. Lefkowitz, Identification of the endophilins (SH3p4/p8/p13) as novel binding partners for the beta1-adrenergic receptor, *Proc Natl Acad Sci USA* **96**, 12559–12564 (1999).
81. A. Mccahill, T. McSorley, E. Huston, E. V. Hill, M. J. Lynch, I. Gall, G. Keryer, B. Lygren, K. Tasken, G. van Heeke, M. D. Houslay, In resting COS1 cells a dominant negative approach shows that specific, anchored PDE4 cAMP phosphodiesterase isoforms gate the activation, by basal cyclic AMP production, of AKAP-tethered protein kinase A type II located in the centrosomal region, *Cell Signal* **17**, 1158–1173 (2005).
82. G. S. Baillie, A. Sood, I. McPhee, I. Gall, S. J. Perry, R. J. Lefkowitz, M. D. Houslay, β -Arrestin-mediated PDE4 cAMP phosphodiesterase recruitment regulates β -adrenoceptor switching from Gs to Gi, *Proc Natl Acad Sci USA* **100**, 940–945 (2003).
83. J. Tao, H.-Y. Wang, C. C. Malbon, Protein kinase A regulates AKAP250 (gravin) scaffold binding to the β 2-adrenergic receptor, *EMBO J* **22**, 6419–6429 (2003).
84. H. Niwa, K. Yamamura, J. Miyazaki, Efficient selection for high-expression transfectants with a novel eukaryotic vector, *Gene* **108**, 193–199 (1991).
85. E. A. Yost, S. M. Mervine, J. L. Sabo, T. R. Hynes, C. H. Berlot, Live cell analysis of G protein β 5 complex formation, function, and targeting, *Mol Pharmacol* **72**, 812–825 (2007).
86. M. L. Dell'Acqua, Membrane-targeting sequences on AKAP79 bind phosphatidylinositol-4,5-bisphosphate, *EMBO J* **17**, 2246–2260 (1998).
87. R. H. Oakley, S. A. Laporte, J. A. Holt, M. G. Caron, L. S. Barak, Differential affinities of visual arrestin, β arrestin1, and β arrestin2 for G protein-coupled receptors delineate two major classes of receptors, *J Biol Chem* **275**, 17201–17210 (2000).
88. M. Zaccolo, T. Pozzan, Discrete microdomains with high concentration of cAMP in stimulated rat neonatal cardiac myocytes, *Science* **295**, 1711–1715 (2002).
89. M. L. Halls, D. P. Poole, A. M. Ellidson, C. J. Nowell, M. Canals, Detection and quantification of intracellular signaling using FRET-based biosensors and high content imaging, *Methods Mol Biol* **1335**, 131–161 (2015).

90. M. L. Halls, C. P. Bond, S. Sudo, J. Kumagai, T. Ferraro, S. Layfield, R. A. D. Bathgate, R. J. Summers, Multiple binding sites revealed by interaction of relaxin family peptides with native and chimeric relaxin family peptide receptors 1 and 2 (LGR7 and LGR8), *J Pharmacol Exp Ther* **313**, 677–687 (2005).
91. K. J. Livak, T. D. Schmittgen, Analysis of relative gene expression data using real-time quantitative PCR and the 2(-Delta Delta C(T)) Method, *Methods* **25**, 402–408 (2001).
92. M. L. Halls, H. R. Yeatman, C. J. Nowell, G. L. Thompson, A. B. Gondin, S. Civciristov, N. W. Bunnett, N. A. Lambert, D. P. Poole, M. Canals, Plasma membrane localization of the μ -opioid receptor controls spatiotemporal signaling, *Sci Signal* **9**, ra16–ra16 (2016).
93. V. O. Nikolaev, M. Bünemann, L. Hein, A. Hannawacker, M. J. Lohse, Novel single chain cAMP sensors for receptor-induced signal propagation, *J Biol Chem* **279**, 37215–37218 (2004).
94. J. Schindelin, I. Arganda-Carreras, E. Frise, V. Kaynig, M. Longair, T. Pietzsch, S. Preibisch, C. Rueden, S. Saalfeld, B. Schmid, J.-Y. Tinevez, D. J. White, V. Hartenstein, K. Eliceiri, P. Tomancak, A. Cardona, Fiji: an open-source platform for biological-image analysis, *Nat Meth* **9**, 676–682 (2012).
95. E. Kardash, J. Bandemer, E. Raz, Imaging protein activity in live embryos using fluorescence resonance energy transfer biosensors, *Nat Protoc* **6**, 1835–1846 (2011).
96. D. A. Sykes, M. R. Dowling, J. Leighton-Davies, T. C. Kent, L. Fawcett, E. Renard, A. Trifilieff, S. J. Charlton, The influence of receptor kinetics on the onset and duration of action and the therapeutic index of NVA237 and tiotropium, *J Pharmacol Exp Ther* **343**, 520–528 (2012).
97. Y. A. Koryakina, T. W. Fowler, S. M. Jones, B. J. Schnackenberg, L. E. Cornett, R. C. Kurten, Characterization of a panel of six β 2-adrenergic receptor antibodies by indirect immunofluorescence microscopy, *Respir Res* **9**, L279 (2008).
98. B. Huang, H. Wu, D. Bhaya, A. Grossman, S. Granier, B. K. Kobilka, R. N. Zare, Counting low-copy number proteins in a single cell, *Science* **315**, 81–84 (2007).
99. P. J. Boersema, R. Raijmakers, S. Lemeer, S. Mohammed, A. J. R. Heck, Multiplex peptide stable isotope dimethyl labeling for quantitative proteomics, *Nat Protoc* **4**, 484–494 (2009).
100. J. Cox, M. Mann, MaxQuant enables high peptide identification rates, individualized p.p.b.-range mass accuracies and proteome-wide protein quantification, *Nat Biotechnol* **26**, 1367–1372 (2008).
101. UniProt Consortium, UniProt: a hub for protein information, *Nucleic Acids Res* **43**, D204–12 (2015).
102. D. W. Huang, B. T. Sherman, R. A. Lempicki, Systematic and integrative analysis of large gene lists using DAVID bioinformatics resources, *Nat Protoc* **4**, 44–57 (2008).
103. D. W. Huang, B. T. Sherman, R. A. Lempicki, Bioinformatics enrichment tools: paths toward the comprehensive functional analysis of large gene lists, *Nucleic Acids Res* **37**, 1–13 (2009).
104. D. Diviani, J. Soderling, J. D. Scott, AKAP-Lbc anchors protein kinase A and nucleates G α 12-selective Rho-mediated stress fiber formation, *J Biol Chem* **276**, 44247–44257 (2001).

105. J. Tao, H.-Y. Wang, C. C. Malbon, Protein kinase A regulates AKAP250 (gravin) scaffold binding to the β 2-adrenergic receptor, *EMBO J* **22**, 6419–6429 (2003).

106. J. A. Vizcaino, A. Csordas, N. del-Toro, J. A. Dianes, J. Griss, I. Lavidas, G. Mayer, Y. Perez-Riverol, F. Reisinger, T. Tement, Q. W. Xu, R. Wang, H. Hermjakob, 2016 update of the PRIDE database and related tools, *Nucleic Acids Res* **44**, D447–D456 (2016).

Acknowledgements: The authors thank Professors Roger J Summers, Dermot MF Cooper, Patrick M Sexton and Arthur Christopoulos for critical discussion, and Mr Cameron J Nowell (Monash Institute of Pharmaceutical Sciences Imaging, Flow Cytometry and Analysis Core Facility), Dr Cheng Huang (Monash Biomedical Proteomics Facility) and Ms Carmen Choo for technical assistance. **Funding:**

This work was supported by a National Health and Medical Research Council of Australia R.D. Wright Fellowship (1061687) and Project Grant (1047633) to M.L.H., a Monash Institute of Pharmaceutical Sciences Strategic Grant to M.L.H., and a NIH/NIGMS grant to WSH (P50GM085273). **Author**

contributions: Conceptualization, M.L.H.; Methodology, R.S., B.A.E., M.L.H.; Formal Analysis, S.C., R.S, M.L.H.; Investigation, S.C., A.M.E., R.S., C.K.P., O.K., S.J.C., W.S.H., M.C., M.L.H.; Writing – Original Draft, M.L.H.; Writing – Review & Editing, S.C., A.M.E., R.S., B.A.E., W.S.H., M.C., M.L.H.; Supervision, A.M.E., O.K., W.S.H., M.C., M.L.H.; Funding Acquisition, M.L.H.

Competing interests: The authors declare that they have no competing interests. **Data and materials**

availability: The mass spectrometry proteomics data have been deposited to the ProteomeXchange Consortium via the PRIDE (106) partner repository with the dataset identifier PXD011033. All data needed to evaluate the conclusions in the paper are present in the paper or the Supplementary Materials.

Figures

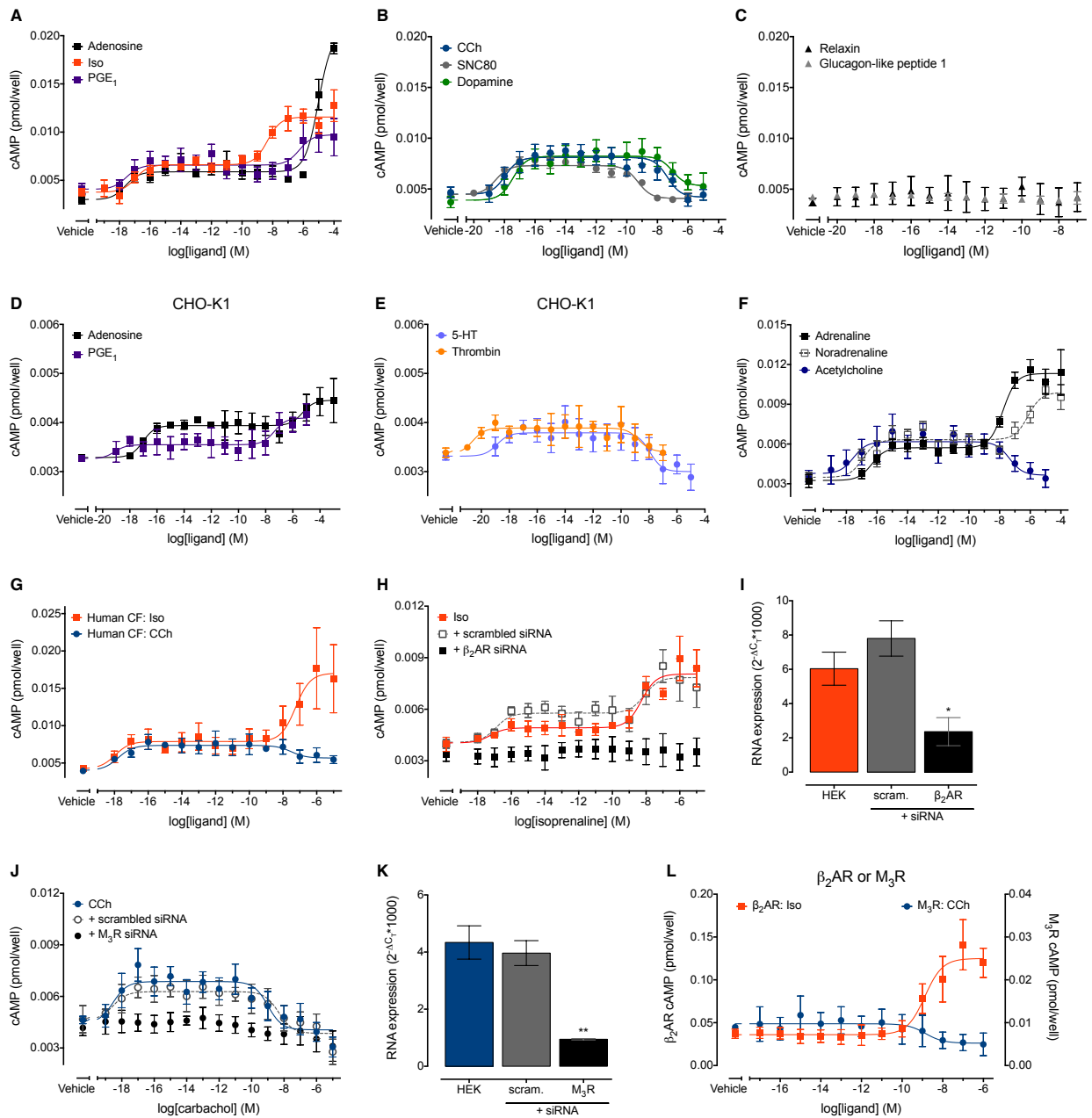


Fig. 1. GPCRs respond to sub-nanomolar concentrations of ligand. (A–C) Quantification of cAMP

in native HEK293 cells stimulated with increasing concentrations of adenosine, the β AR agonist

isopreterenol (Iso), or prostaglandin E₁ (PGE₁) (A); the muscarinic acetylcholine receptor agonist

carbachol (CCh), the delta opioid receptor agonist SNC80, or dopamine (B); and relaxin or glucagon-

like peptide 1 (C) in the absence of the PDE inhibitor IBMX. (n=6-9 independent experiments) (see

also Table S1). **(D–E)** Quantification of cAMP in native CHO-K1 cells stimulated with increasing concentrations of adenosine or PGE₁ (D) and 5-hydroxytryptamine (5-HT) or thrombin (E) in the presence of IBMX. (n=6 independent experiments). **(F)** Quantification of cAMP in native HEK293 cells stimulated with increasing concentrations of adrenaline, noradrenaline or acetylcholine in the absence of IBMX. (n=6-8 independent experiments) (see also Table S1). **(G)** Quantification of cAMP in primary human cardiac fibroblasts (CFs) stimulated with increasing concentrations of Iso or CCh in the absence of IBMX. (n=5-6 independent experiments). **(H)** Quantification of cAMP in native HEK293 cells or HEK293 cells transiently expressing scrambled or β_2AR siRNA, stimulated with increasing concentrations of Iso in the absence of IBMX. (n=6 independent experiments). **(I)** Expression of β_2AR mRNA in native HEK293 cells or HEK293 cells transiently expressing scrambled (scram.) or β_2AR siRNA as determined by qRT-PCR. (n=3 independent experiments). **(J)** Quantification of cAMP in native HEK293 cells or HEK293 cells transiently expressing scrambled or M₃R siRNA, stimulated with increasing concentrations of CCh in the absence of IBMX. (n=6 independent experiments). **(K)** Expression of M₃R mRNA in native HEK293 cells or HEK293 cells transiently expressing scrambled (scram.) or M₃R siRNA as determined by qRT-PCR. (n=3 independent experiments). **(L)** Quantification of cAMP in HEK293 cells transiently expressing the β_2AR or M₃R and stimulated with increasing concentrations of Iso or CCh, respectively, in the absence of IBMX (n=3-4 independent experiments). All data are expressed as the mean \pm S.E.M. of n independent experiments. * p<0.05 and ** p<0.01 versus HEK293 controls, one-way ANOVA with Tukey's multiple comparison test.

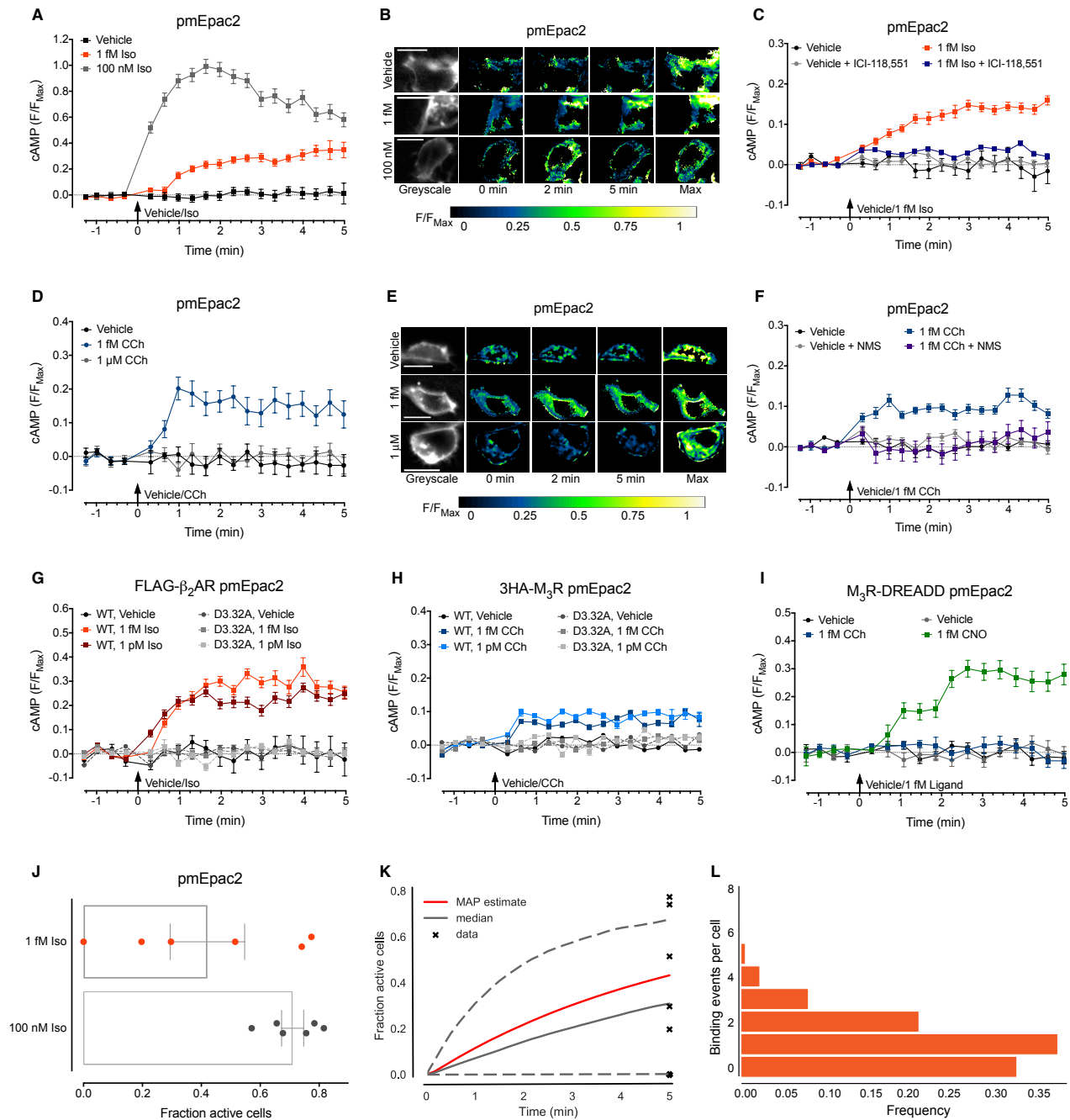


Fig. 2. Femtomolar concentrations of ligand cause sustained increases in plasma membrane-localized cAMP and require an intact orthosteric binding site and only one binding event per cell.

(A) Measurement of cAMP at the plasma membrane in single native HEK293 cells using the FRET biosensor, pmEpac2, which reversibly binds cAMP. Cells were stimulated with vehicle, 1 fM Iso, or 100 nM Iso. (n=47-79 cells). (B) Representative ratiometric pseudocolor images of cells from (A) at

the indicated time points following stimulation. Scale bar, 10 μm . (C) Measurement of cAMP at the plasma membrane in single native HEK293 cells pre-incubated with the $\beta_2\text{AR}$ antagonist ICI-118,551 before stimulation with vehicle or 1 fM Iso. (n=51-97 cells). (D) Measurement of cAMP at the plasma membrane in single native HEK293 cells stimulated with vehicle, 1 fM CCh, or 1 μM CCh. n=29-53 cells. (E) Representative ratiometric pseudocolor images of cells from (D) at the indicated time points following stimulation. Scale bar, 10 μm (F) Measurement of cAMP at the plasma membrane in single native HEK293 cells pre-incubated with the M_3R antagonist N-methyl scopolamine (NMS) before stimulation with vehicle or 1 fM CCh. (n=56-95 cells). (G) Measurement of cAMP at the plasma membrane in single HEK293 cells transiently expressing wild-type (WT) FLAG- $\beta_2\text{AR}$ or the orthosteric binding site D3.32A mutant FLAG- $\beta_2\text{AR}$ and stimulated with vehicle, 1 fM Iso, or 1 pM Iso. (n=43-151 cells). (H) Measurement of cAMP at the plasma membrane in single HEK293 cells transiently expressing WT or D3.32A mutant 3HA- M_3R and stimulated with vehicle, 1 fM CCh, or 1 pM CCh. (n=119-186 cells). (I) Measurement of cAMP at the plasma membrane in single HEK293 cells transiently expressing M_3R -DREADD and stimulated with vehicle, 1 fM CCh, or 1 fM CNO. (n=57-89 cells). All cells were stimulated at 0 min, and a maximal cAMP response (Max.) was induced after 5 min by stimulating the cells with forskolin, IBMX, and PGE_1 . Individual cells were analyzed from experiments performed on three independent occasions. Data are expressed as the mean \pm S.E.M. of n cells, normalized to the maximal cAMP response induced after 5 min (F/F_{Max}). (J) Fraction of HEK293 cells within the field of view that increased cAMP at the plasma membrane following a 5 min exposure to 1 fM or 100 nM Iso. Data were analyzed from experiments in Fig. 3, A and B, with an area under the curve (AUC) of greater than 0.697 considered significantly increased compared to vehicle control. Data are expressed as the mean \pm S.E.M. of 6 independent experiments. (K) The 95% credible interval for responses to 1 fM Iso over 5 min, using 1,000 randomly subsampled parameter sets from the MCMC sampling procedure. The red line shows the time course with parameters consistent with

the maximum *a posteriori* probability (MAP) estimate. The solid grey line shows the median, and the dashed grey lines show the 95% credible interval for the sub-sampled parameter sets. The 1 fM Iso data from (J) is shown as crosses; for two of these only a small region (~2%) of sampled parameter space allows the model to reach these points. (L) Normalized frequency of binding for 1 fM Iso from 100 independent model simulations with the MAP estimate parameter set. The average number of binding events is 1.13 per cell.

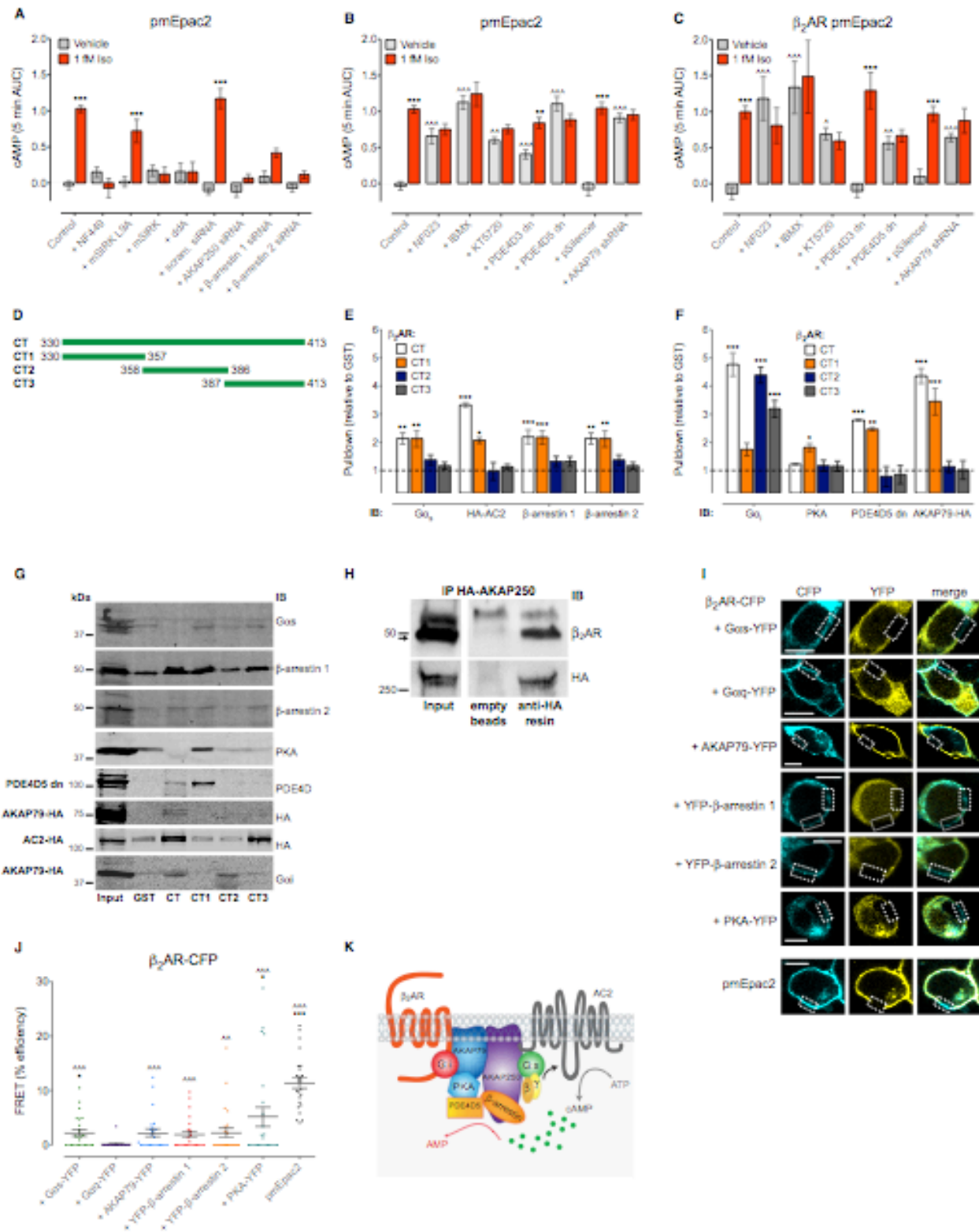


Fig. 3. A pre-assembled β_2 AR signaling complex controls the response to femtomolar concentrations of ligand. (A) Measurement of cAMP at the plasma membrane in response to 5 min of

stimulation with vehicle or 1 fM Iso in single native HEK293 cells that were pre-treated with the $G\alpha_s$ antagonist NF449, the $G\beta\gamma$ inhibitor mSIRK, the negative control peptide mSIRK L9A, or the AC inhibitor 2',5'-dideoxyadenosine (ddA) or transient expression of scrambled (scram.), AKAP250, β -arrestin 1, or β -arrestin 2 siRNA. (n=36-254 cells). **(B)** Measurement of cAMP at the plasma membrane in response to 5 min of stimulation with vehicle or 1 fM Iso in single native HEK293 cells were pre-treated with the $G\alpha_{i/o}$ antagonist NF023, the PDE inhibitor IBMX, or the PKA inhibitor KT5720 or transient expression of PDE4D3 dominant negative (dn), PDE4D5 dn, pSilencer control, or AKAP79 shRNA. (n=22-254 cells). **(C)** Measurement of cAMP at the plasma membrane following 5 min of stimulation with vehicle or 1 fM Iso in HEK293 cells transiently expressing the β_2 AR. Cells were pre-treated with the $G\alpha_{i/o}$ antagonist NF023, the PDE inhibitor IBMX, or the PKA inhibitor KT5720 or transient coexpression of PDE4D3 dn, PDE4D5 dn, pSilencer control, or AKAP79 shRNA. (n=22-153 cells). All cells (A–C) were stimulated at 0 min, and a maximal cAMP response (Max.) was induced after 5 min by the addition of forskolin, IBMX, and PGE_1 . Individual cells were analyzed from experiments performed on three independent occasions. Data are expressed as the mean \pm S.E.M. of n cells and represented as the 5 min area under the curve (AUC). *** $p < 0.001$ versus vehicle control, two-way ANOVA with Sidak's multiple comparison test; ^^ $p < 0.01$ and ^^ $p < 0.001$ versus untreated control, two-way ANOVA with Dunnett's multiple comparison test. **(D)** Cartoon showing the regions of the β_2 AR C-terminal tail (CT) that were tagged with GST. **(E)** Quantification of proteins identified as required for activation of cAMP in response to 1 fM Iso in GST pulldowns from lysates of unstimulated native HEK293 cells using the indicated CT-GST fusions. GST pulldowns were assayed for endogenous $G\alpha_s$ (short and long forms), transgenically expressed HA-AC2, endogenous β -arrestin 1, and endogenous β -arrestin 2. (n=5-6). **(F)** Quantification of proteins identified as required for regulation of constitutive activity of the pre-assembled β_2 AR complex in GST pulldowns from lysates of unstimulated native HEK293 cells using the indicated CT-GST fusions. GST pulldowns were

assayed for endogenous $G\alpha_i$ (in cells transgenically expressing AKAP79-HA), endogenous PKA, transgenically expressed PDE4D5 dn, and transgenically expressed AKAP79-HA. (n=3-4). For GST pulldown assays (E–F), band densities were normalized for equivalent amounts of GST and expressed relative to GST alone. Data are mean \pm S.E.M. of n independent experiments. * $p < 0.05$ and *** $p < 0.001$ versus GST alone, two-way ANOVA with Dunnett’s multiple comparison test. **(G)** Representative immunoblots (IB) showing $G\alpha_s$, β -arrestin 1, β -arrestin 2, PKA, PDE4D, HA and $G\alpha_i$ in GST pulldown assays of lysates from cells using GST alone or the indicated CT-GST fusions. **(H)** Representative immunoblots showing β_2 AR and HA following HA immunoprecipitation (IP) of lysates from HEK293 cells transiently expressing HA-AKAP250. **(I)** Representative images of cells co-expressing β_2 AR-CFP and a YFP-tagged component of the β_2 AR-associated complex or the positive control pmEpac2, following acceptor photobleaching of a region of the plasma membrane (dotted box). Grey solid boxes indicate areas of the plasma membrane that were photobleached previously. Scale bar, 10 μ m. **(J)** FRET efficiency at the plasma membrane between β_2 AR-CFP and YFP-tagged components of the protein complex, calculated from acceptor photobleaching FRET experiments from two regions of interest (ROI) per cell with four cells analyzed per biological replicate. (n=24 ROIs). Data are expressed as the mean \pm S.E.M. of n ROIs. * $p < 0.05$ and *** $p < 0.001$ versus β_2 AR-CFP/ $G\alpha_q$ -YFP FRET efficiency, Kruskal-Wallis with Dunn’s multiple comparison test; ^^ $p < 0.01$ and ^^ ^ $p < 0.001$ versus β_2 AR-CFP/ $G\alpha_q$ -YFP FRET following conversion to binary values (1 = FRET, 0 = no FRET) then Chi-square test. **(K)** Cartoon of the pre-assembled β_2 AR signaling complex required for responses to femtomolar concentrations of Iso. Stimulation of cells with 1 fM Iso activates a $G\alpha_s$ and $G\beta\gamma$ -mediated stimulation of AC2 that depends on AKAP250 and β -arrestins 1 and 2. This increase in cAMP causes the sequential activation of PKA and PDE4D5, which cooperates with $G\alpha_{i/o}$ to oppose the increase in cAMP. This tonic opposition depends on AKAP79. Hierarchy of proteins within the

cartoon is based on whether proteins mediate activation or inhibition and reported protein-protein interactions (3, 5, 53, 59, 104, 105).

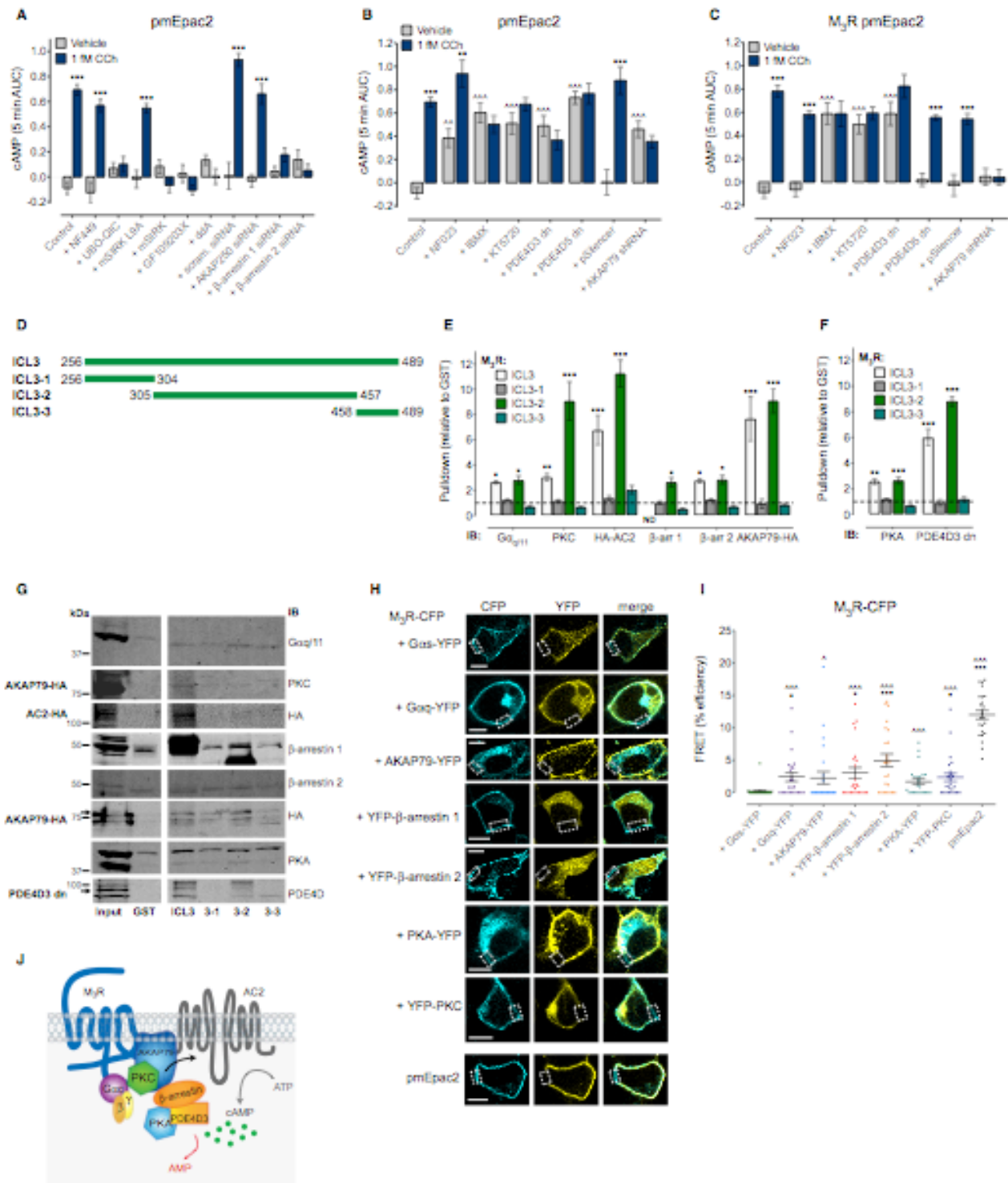


Fig. 4. A pre-assembled M₃R signaling complex controls the response to femtomolar concentrations of ligand. (A) Measurement of cAMP at the plasma membrane in response to 5 min of stimulation with vehicle or 1 fM CCh in single native HEK293 cells that were pre-treated with the G α_s antagonist NF449, the G $\alpha_{q/11}$ inhibitor UBO-QIC, the G $\beta\gamma$ inhibitor mSIRK, the negative control

peptide mSIRK L9A, the PKC inhibitor GF109203X, or the AC inhibitor 2',5'-dideoxyadenosine (ddA) or transiently transfected with scrambled (scram.), AKAP250, β -arrestin 1 or β -arrestin 2 siRNA. (n=39-316 cells). **(B)** Measurement of cAMP at the plasma membrane in response to 5 min of stimulation with vehicle or 1 fM CCh in single native HEK293 cells that were pre-treated with the $G\alpha_{i/o}$ antagonist NF023, the PDE inhibitor IBMX, or the PKA inhibitor KT5720 or transiently transfected with PDE4D3 dn, PDE4D5 dn, pSilencer control, or AKAP79 shRNA. (n=31-316 cells). **(C)** Measurement of cAMP at the plasma membrane following 5 min of stimulation with vehicle or 1 fM CCh in HEK293 cells transiently expressing the M_3R . Cells were pre-treated with the $G\alpha_{i/o}$ antagonist NF023, the PDE inhibitor IBMX, or the PKA inhibitor KT5720 or transiently co-transfected with PDE4D3 dn, PDE4D5 dn, pSilencer control, or AKAP79 shRNA. (n=65-193 cells). All cells (A–C) were stimulated at 0 min, and a maximal cAMP response (Max.) was induced after 5 min with forskolin, IBMX, and PGE_1 . Individual cells were analyzed from experiments performed on three independent occasions. Data are expressed as the mean \pm S.E.M. of n cells, and represented as the 5 min area under the curve (AUC). ** $p < 0.01$ and *** $p < 0.001$ versus vehicle control, two-way ANOVA with Sidak's multiple comparison test; ^^ $p < 0.01$ and ^^ ^ $p < 0.001$ versus untreated control, two-way ANOVA with Dunnett's multiple comparison test. **(D)** Cartoon showing the regions of the M_3R third intracellular loop (ICL3) that were tagged with GST. **(E)** Quantification of proteins required for activation of cAMP in response to 1 fM CCh in GST pulldowns from unstimulated native HEK293 cells using the indicated ICL3-GFP fusions. GST pulldowns were assayed for endogenous $G\alpha_{q/11}$, endogenous PKC (from cells transgenically expressing with AKAP79-HA), transgenically expressed HA-AC2, endogenous β -arrestin 1, endogenous β -arrestin 2 and transgenically expressed AKAP79-HA (n=3-4). **(F)** Quantification of GST pulldowns from unstimulated native HEK293 cell lysates of proteins required for regulation of constitutive activity of the pre-assembled M_3R complex: endogenous PKA and transgenically expressed PDE4D3 dn (n=3-4). For GST pulldown assays, band densities were

normalized for equivalent amounts of GST, and expressed relative to GST alone. Data are mean \pm S.E.M. of n independent experiments. * $p < 0.05$, ** $p < 0.01$ and *** $p < 0.001$ versus GST alone, two-way ANOVA with Dunnett's multiple comparison test. **(G)** Representative immunoblots (IB) showing $G\alpha_{q/11}$, PKC, HA, β -arrestin 1, β -arrestin 2, PKA, and PDE4D in GST pulldown assays of lysates using GST alone or the indicated ICL3-GST fusions. **(H)** Representative images of cells co-expressing M_3R -CFP and a YFP-tagged component of the M_3R protein complex or the positive control pmEpac2, following acceptor photobleaching of a region of the plasma membrane (dotted box). Scale bar, 10 μ m. **(I)** FRET efficiency at the plasma membrane between M_3R -CFP and YFP-tagged components of the protein complex, calculated from acceptor photobleaching FRET experiments from two regions of interest (ROI) per cell with four cells analyzed per biological replicate (n=24 ROIs). Data are expressed as the mean \pm S.E.M. of n ROIs. * $p < 0.05$ and *** $p < 0.001$ versus M_3R -CFP/ $G\alpha_s$ -YFP FRET efficiency, Kruskal-Wallis with Dunn's multiple comparison test; ^ $p < 0.05$ and ^^ $p < 0.001$ versus M_3R -CFP/ $G\alpha_s$ -YFP FRET following conversion to binary values (1 = FRET, 0 = no FRET) then Chi-square test. **(J)** Cartoon of the pre-assembled M_3R signaling complex required for responses to femtomolar concentrations of CCh. Stimulation of cells with 1 fM CCh activates a $G\alpha_{q/11}$ - $G\beta\gamma$ -PKC-mediated stimulation of AC2 that depends on AKAP79 and β -arrestins 1 and 2. This increase in cAMP causes the sequential activation of PKA and PDE4D3, which opposes the increase in cAMP. Hierarchy of proteins within the cartoon is based on reported protein-protein interactions (5, 55, 63).

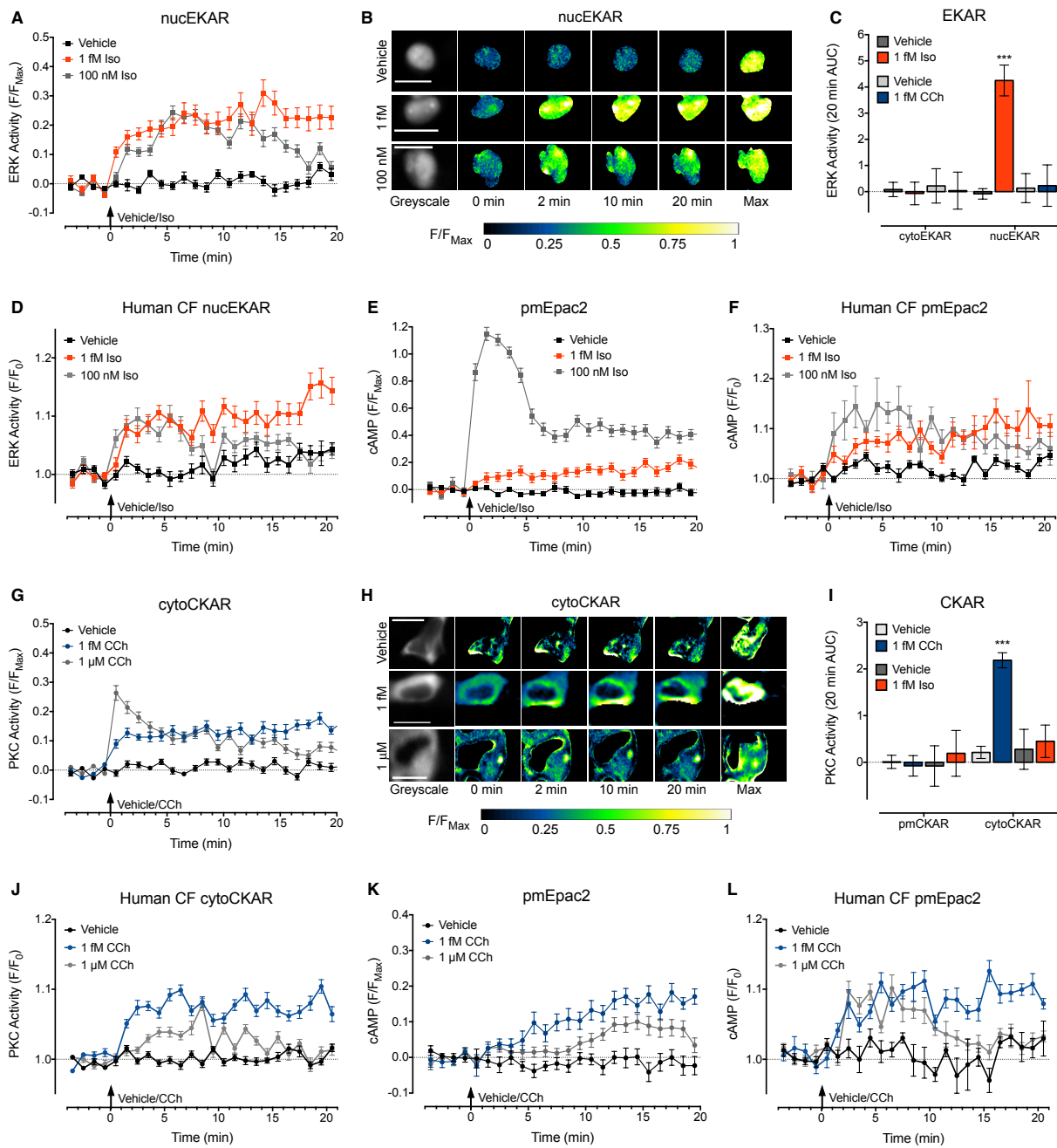


Fig. 5. Stimulation of the β_2 AR and M_3 R by femtomolar concentrations of ligand activates

sustained and compartmentalized kinase signaling. (A–F) Single native cells were stimulated with

vehicle, or the indicated concentration of Iso for 20 min. (A) ERK activity detected in the nucleus of

HEK293 cells using the FRET biosensor, EKAR, which is reversibly phosphorylated by ERK and

targeted to the nucleus (nucEKAR). (n=118-133 cells). Data are normalized to the maximal ERK

response (F/F_{Max}). (B) Representative ratiometric pseudocolor images of cells from (A) at the indicated

time points following stimulation. Scale bar, 10 μm (C) ERK activity detected in the cytosol using the cytoEKAR FRET biosensor or nucleus (nucEKAR) of HEK293 cells. Some cells were stimulated with 1 fM CCh instead of Iso for 20 min. (n=13-130 cells). Data is represented as the 20 min area under the curve (AUC). (D) ERK activity detected in the nucleus of human cardiac fibroblasts (CFs). (n=38-61 cells). Data are normalized to the baseline ERK response (F/F_0). (E) cAMP detected at the plasma membrane in HEK293 cells. (n=31-44 cells). Data are normalized to the maximal cAMP response induced after 20 min (F/F_{Max}). (F) cAMP detected at the plasma membrane of human CFs. (n=22-53 cells). Data are normalized to the baseline cAMP response (F/F_0). (G-L) Single native cells were stimulated with vehicle or the indicated concentration of CCh for 20 min. (G) PKC activity detected in the cytosol of HEK293 cells using the FRET biosensor, CKAR, which is reversibly phosphorylated by PKC. (n=185-226 cells). Data are normalized to the maximal PKC response induced after 20 min (F/F_{Max}). (H) Representative ratiometric pseudocolor images of cells from (G) at the indicated time points following stimulation. Scale bar, 10 μm (I) PKC activity detected at the plasma membrane (pmCKAR) or in the cytosol (cytoCKAR) of HEK293 cells. Some cells were stimulated with 1 fM Iso instead of CCh. (n=10-175 cells). Data is represented as the 20 min AUC. (J) PKC activity detected in the cytosol of human CFs. (n=69-124 cells). Data are normalized to the baseline PKC response (F/F_0). (K) cAMP detected at the plasma membrane of HEK293 cells. (n=32-44 cells). Data are normalized to the maximal cAMP response induced after 20 min (F/F_{Max}). (L) cAMP detected at the plasma membrane of human CFs. (n=31-50 cells). Data are normalized to the baseline cAMP response (F/F_0). All cells were stimulated at 0 min, and a maximal ERK, PKC, or cAMP response (Max.) was induced after 20 min with PDBu (ERK), PDBu plus phosphatase inhibitors (PKC), or forskolin plus IBMX and PGE₁ (cAMP). Individual cells were analyzed from experiments performed on three independent occasions. Data are expressed as the mean \pm S.E.M. of n cells. *** $p < 0.001$ versus vehicle control, two-way ANOVA with Sidak's multiple comparison test.

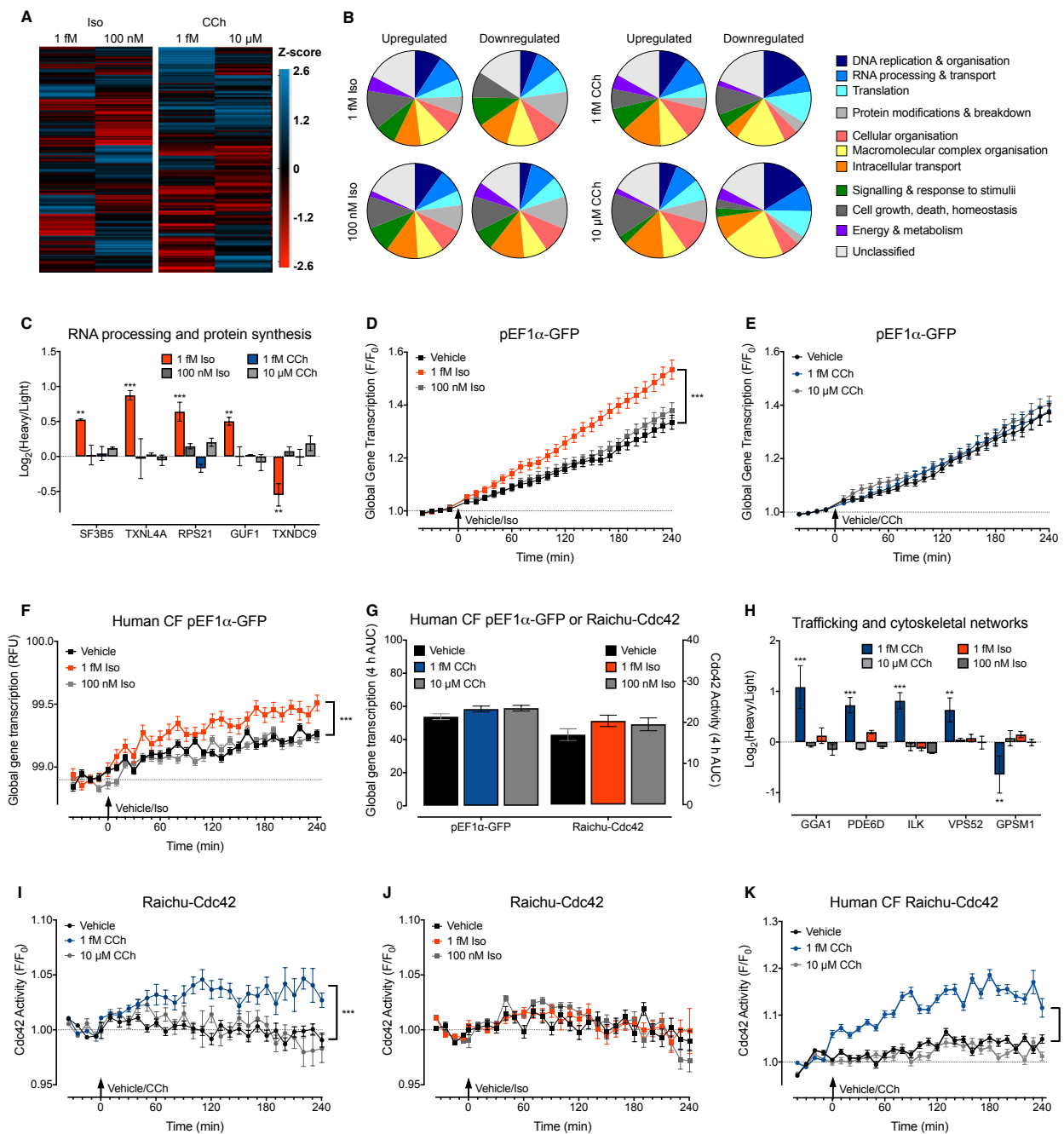


Fig. 6. Activation of the β_2 AR and M_3 R by femtomolar concentrations of ligand causes distinct whole cell responses. (A) Representative hierarchical clustering of proteins with increased (blue) or decreased (red) abundance in native HEK293 cell populations following stimulation with vehicle, 1 fM or 100 nM Iso, or 1 fM or 10 μ M CCh for 4 h. Data are expressed as Z-scores of the ligand-stimulated

change in protein abundance compared to vehicle (see also Table S3). (from n=3 independent experiments). **(B)** Proteins with a significant increase or decrease in abundance in native HEK293 cells following stimulation with Iso or CCh were classified by Gene Ontology (GO) terms and grouped into the indicated categories. A GO biological process term was included if it occurred in at least two out of the three independent experiments. **(C)** Log₂ change in protein abundance in the indicated native HEK293 treatment groups versus vehicle control for SF3B5, TXNL4A, RPS21, GUF1, and TXNDC9, all of which are involved in RNA processing and protein synthesis. (n=3). **(D-E)** GFP fluorescence in single native HEK293 cells expressing the pEF1 α -GFP reporter following stimulation with vehicle, 1 fM or 100 nM Iso (D; n=196-204 cells), or 1 fM or 10 μ M CCh (E; 177-194 cells) for 4 h. Individual cells were analyzed from three independent experiments. Data are expressed relative to baseline fluorescence (F/F₀). **(F)** GFP fluorescence in single human cardiac fibroblasts (CF) expressing the pEF1 α -GFP reporter following stimulation with vehicle, 1 fM Iso, or 100 nM Iso for 4 h. (n=64-107 cells). Individual cells were analyzed from four independent experiments. Data are expressed as relative fluorescence units (RFU) per cell. **(G)** GFP fluorescence in single human CFs expressing the pEF1 α -GFP reporter following stimulation with vehicle, 1 fM CCh, or 10 μ M CCh (n=109-121 cells), and activation of Cdc42, as measured by the Raichu-Cdc42 FRET biosensor which detects GDP/GTP binding, in single human CFs following stimulation with vehicle, 1 fM Iso, or 100 nM Iso (n=133-178 cells) expressed as the 4 h area under the curve (AUC). **(H)** Log₂ change in protein abundance in the indicated native HEK293 treatment groups versus vehicle control for GGA1, PDE6D, ILK, VPS52, and GPSM1, all of which are involved in protein trafficking and cytoskeletal networks. (n=3). **(I-J)** Activation of Cdc42 in single native HEK293 cells following stimulation with vehicle, 1 fM or 10 μ M CCh (I; n=305-323 cells), or 1 fM or 100 nM Iso (J; n=304-401 cells) for 4 h. Individual cells were analyzed from three independent experiments. Data are expressed relative to baseline FRET (F/F₀). **(K)** Activation of Cdc42 in single human CFs following stimulation with vehicle, 1 fM CCh, or 10 μ M

CCh for 4 h. (n=150-159 cells). Individual cells were analyzed from three independent experiments. Data are expressed relative to baseline FRET (F/F_0). All data are expressed as the mean \pm S.E.M. of n cells or independent experiments. * $p < 0.05$ and ** $p < 0.01$ versus vehicle control, two-way ANOVA with Dunnett's multiple comparison test (C, H). *** $p < 0.001$ versus vehicle control, two-way ANOVA (D, F, I, K).

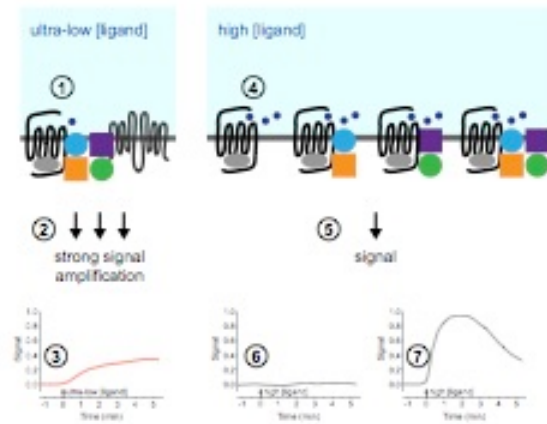


Fig. 7. GPCR signaling complexes respond to femtomolar concentrations of ligand. GPCRs exist in pre-assembled protein complexes at the plasma membrane. (1) Simulation of stochastic ligand-receptor binding kinetics reveals that the addition of a 1 fM solution of ligand under our assay conditions would result in an average of one to two binding events per cell within 5 min. (2) One–two binding events stimulates strong signal amplification, which depends on a pre-assembled protein complex at the plasma membrane and results in (3) a relatively slow and gradual increase in the signal over time. (4) Addition of a high concentration solution of ligand (100 nM Iso or 1 μ M CCh) results in a much greater number of binding events and activates receptors that are present in pre-assembled complexes as well as any uncomplexed receptors. (5) The resulting activation stimulates a signal that is qualitatively different from that elicited by ultra-low ligand concentrations, such as (6) no signal (CCh-stimulated cAMP, EF1 α gene transcription, or Cdc42 activity) or (7) a more rapid increase in the signal that then declines (Iso-stimulated cAMP, nuclear ERK, or cytosolic PKC).